THE PENNSYLVANIA STATE UNIVERSITY
SCHREYER HONORS COLLEGE

DEPARTMENT OF ASTRONOMY & ASTROPHYSICS

INVESTIGATIONS OF SHORT-TIMESCALE C IV BROAD ABSORPTION LINE VARIABILITY

ZACHARY S. HEMLER
SUMMER 2018

A thesis
submitted in partial fulfillment
of the requirements
for a baccalaureate degree
in Astronomy & Astrophysics
with honors in Astronomy & Astrophysics

Reviewed and approved* by the following:

William Nielsen Brandt
Verne M. Willaman Professor of Astronomy & Astrophysics
Professor of Physics
Thesis Supervisor

Steinn Sigurðsson
Professor of Astronomy & Astrophysics
Honors Adviser

*Signatures are on file in the Schreyer Honors College.

Abstract

We systematically investigate significant, short-timescale (<10-day rest-frame) C IV broad absorption-line (BAL) variability to constrain quasar-wind properties and provide insights into BAL variability mechanisms in quasars. We employ data taken by the Sloan Digital Sky Survey Reverberation Mapping (SDSS-RM) project, as the rapid cadence of these observations provides a novel opportunity to examine BAL variability on shorter rest-frame timescales than have previously been explored. In a sample of 27 quasars with a median of 58 spectral epochs per quasar, we have identified 54 epoch pairs exhibiting significant C IV BAL equivalent width variability on timescales of less than 10 days in the quasar rest frame. This rapid variability is observed in $55^{+18}_{-14}\%$ of the quasar sample, indicating that such variability is common among quasars. We examine a variety of characteristics of the spectra, such as the presence of other species that indicate likely C IV saturation, and search for coordinated BAL variability across a range of velocities. We find that in some cases, the evidence is supportive of the observed variability being driven by ionization state variability, while in other cases the evidence is more consistent with models involving changes in covering fraction or density. This is the first study to analyze BAL variability in a sample of quasars on such short timescales, and the high incidence of rapid variability in the sample suggests that models describing BALs and their behavior must account for variability on timescales down to less than a day in the quasar rest frame.

Table of Contents

List of Figures

List of Tables

Chapter 1

Introduction

1.1 Quasar Outflows

One of the major questions driving studies of galaxy evolution is the nature of the interaction between galaxies and their central supermassive black holes (SMBHs). A possible avenue for this interaction is through quasar outflows, or winds, generated near the SMBH (e.g., Di Matteo et al., 2005; Moll et al., 2007; King & Pounds, 2015). Quasar outflows are launched from the accretion disk around the SMBH (e.g., Murray et al., 1995; Proga, 2000; Higginbottom et al., 2014), and are thought to regulate the growth of the host galaxy, and the SMBH itself, through the process of AGN feedback. Specifically, outflows provide a mechanism for a host-galaxy to evacuate gas, can slow or stop SMBH accretion, and can enhance or suppress host-galaxy star formation. Understanding the physical properties of these outflows is thus integral to developing models of active galaxy evolution. In the context of rest-frame UV quasar spectra, these outflows manifest themselves as broad absorption lines (BALs), features that exhibit observed velocity widths on the scale of several thousand km s^{-1} (Weymann et al. 1991). BALs are an extremely useful probe of outflow physical properties, as well as the environments from which they originate.

Previous studies have demonstrated that BALs are significantly variable, both in strength and in shape (e.g., Barlow, 1993; Lundgren et al., 2007; Gibson et al., 2008; Filiz Ak et al., 2013; Capellupo et al., 2013). Proposed mechanisms for BAL variability include inhomogeneous emission, ionization-state changes, and "cloud crossing", which refers to the drift of the absorbing gas across the line of sight (e.g., Hall et al., 2007; Capellupo et al., 2013; Filiz Ak et al., 2013). Characterizing the variations of BALs can yield constraints for many physical properties of quasar outflows; for example, ionization-state changes and cloud-crossing allow an inference of the density and/or radial distance of the relevant gas from the SMBH (e.g., Capellupo et al., 2013).

1.2 BAL Variability Investigations

While BAL variability has been commonly studied on rest-frame timescales of years and months (e.g., Gibson et al., 2010), observations probing timescales of days and hours are rare (e.g., Capellupo et al., 2013; Grier et al., 2015). Moreover, most studies have suffered a trade-off between the numbers of observed quasars and the number of observations. For this reason, there has not yet been a study with both the sample size and rapid cadence required to make robust statistical statements about variability on timescales on the orders of days to tens of days in the quasar rest frame. Table 1.1 presents the sample characteristics of several prior BAL-variability studies for the purposes of comparison to this investigation.

Spectroscopic data from the Sloan Digital Sky Survey Reverberation Mapping program (SDSS-RM; Shen et al., 2015) provide a novel opportunity to investigate BAL variability on shorter timescales than have previously been explored in a large sample of quasars using many epochs of spectra. The SDSS-RM project is an ongoing reverberation mapping campaign that began in 2014 and has continued to obtain data in subsequent years during January – July of each year. Many quasars in the SDSS-RM quasar sample exhibit BAL features in their spectra. Prior to this program, the shortest BAL-variability timescales probed were on the order of 8–10 days (Capellupo et al. 2013). However, with the rapid cadence of the SDSS-RM dataset, Grier et al. (2015) were able to probe even shorter timescales: They identified significant variability of a C IV BAL on timescales as short as 1.2 days in the quasar rest frame. On these short timescales, the equivalent

Table 1.1. Parameters of BAL Variability Studies

Reference	No. of Quasars	$N_{\rm epochs}$[a] Range	Median $N_{\rm epochs}$[a]	$\Delta t_{\rm rest}$[b] Range (days)	Median $\Delta t_{\rm rest}$[b](days)	Redshift Range	Median Redshift
Barlow (1993)	23	2–6	···	73–440	···	···	···
Lundgren et al. (2007)	29	2	2	18–121	81	1.70–3.26	2.00
Gibson et al. (2008)	13	2	2	1100–2200	1500	1.72–2.81	2.02
Gibson et al. (2010)	14	2–4	3	15–2500	1100	2.08–2.89	2.41
Capellupo et al. (2011)	24	2–4	4	130–2800	1600	1.22–2.91	2.23
Capellupo et al. (2012)	24	2–10	5	15–3000	270	1.22–2.91	2.23
Vivek et al. (2012)	5	4–14	5	3.7–1200	140	0.81–1.97	1.23
Haggard et al. (2012)	17	6	···	0.37–330	···	···	···
Filiz Ak et al. (2012)	19	2–4	2	400–1400	730	1.71–2.57	2.00
Capellupo et al. (2013)	24	2–13	7	7.3–3200	270	1.22–2.91	2.23
Welling et al. (2014)	46	2–6	2	80–6000	500	0.24–3.46	2.21
Filiz Ak et al. (2013)	291	2–12	2	0.22–1350	770	2.00–3.93	2.55
Filiz Ak et al. (2014)	671	2	2	310-1500	930	1.90–3.83	2.28
This work	27	3–68	58	0.21–250	2.4	1.62–3.72	2.35

[a]$\rm N_{epochs}$ refers to the number of epochs *per quasar*.

[b]Δt is measured in the quasar rest-frame.

width of this BAL varied by roughly 10%. Because the BAL showed little variability in shape, Grier et al. (2015) proposed that this feature was likely varying via ionization-state changes in the absorbing medium. This discovery of such short-timescale variability motivates subsequent investigations to determine whether this variability is common among BAL quasars.

In this work, we present the results of a search for short-timescale variability within a sample of BAL quasars using the data from the SDSS-RM program. The goals of this study are to determine the frequency of short-timescale BAL variability, further constrain quasar-wind properties in BAL quasars with significant short-timescale variability, and provide insights into quasar-wind variability mechanisms. Chapter 2 presents the SDSS-RM observations and characterizes our quasar sample. Chapter 3 describes data processing, the measured BAL parameters such as equivalent widths, mean depths, and centroid velocities, and our criteria for selecting robust cases of BAL variability. Chapter 4 discusses our results, our investigations of coordinated variability, and the implications of our work. Chapter 5 summarizes our findings and elaborates on feasible future work in regards to short-timescale BAL variability studies. Where necessary, we adopt a cosmology with $H_0 = 70$ km s^{-1} Mpc^{-1} , $\Omega_M = 0.3$, and $\Omega_\Lambda = 0.7$ (following Schneider et al. 2010).

Chapter 2

Observations & Data Preparation

2.1 SDSS-RM Observations

In 2014, SDSS-RM obtained 32 epochs of spectra of 849 quasars using the Baryon Oscillation Spectroscopic Survey (BOSS; Eisenstein et al., 2011; Dawson et al., 2013) spectrograph on the SDSS 2.5-meter telescope (Gunn et al., 2006; Smee et al., 2013); 12–13 additional epochs per year were taken subsequently in 2015, 2016, and 2017 as a part of the SDSS-IV eBOSS program (Dawson et al. 2016; Blanton et al. 2017), yielding a total of 69 epochs of spectroscopy over the four years. The BOSS spectrograph covers a wavelength range of 3650 – 10,400 Å, has a spectral resolution of R = 2000, and has a field of view that is 3 degrees in diameter. At the beginning of the SDSS-RM program, all 850 quasars were assigned numeric identifiers relating to their position on the spectrograph plate — we hereafter refer to these identification numbers as the RM ID, and refer to all SDSS-RM quasars by this designation.

2.2 Initial Quasar Sample

We began with a parent sample of 94 quasars in the SDSS-RM sample that were identified to likely host prominent C IV absorption features, each with 69 epochs of data from the four years of SDSS-RM monitoring. This initial sample was chosen by visual inspection, and thus may contain C IV absorbers that do not meet the formal requirements for BALs. We later refine our sample to include only those quasars containing BALs as formally defined by Weymann et al. 1991; see Section 3.1. Figure 2.1 shows the absolute magnitude-redshift distribution of our parent quasar sample compared to the general population of quasars from the DR14 quasar catalog (Pâris et al. 2018). The quasars in our parent sample are typical for BAL quasars within the magnitude/redshift plane.

2.3 Data Preparation

The data were first processed using the standard BOSS spectroscopic reduction pipeline; however, to further improve the spectrophotometric flux calibrations of the data, a custom flux calibration scheme was applied to the data (Shen et al., 2015). We then corrected the spectra for Galactic extinction using an R_V = 3.1 Milky Way extinction model (Cardelli et al. 1989) and A_V values from Schlafly & Finkbeiner (2011).

We searched for pixels with poor sky subtraction residuals using the SDSS bitmask flag "BRIGHTSKY" and replaced these pixels using linear interpolation. This process suppressed much of the mid-optical sky contamination in the spectra, although significant sky contamination residuals are still visible at the far red and blue ends of the spectra. There were a few spectra with additional bad pixels that were not flagged by SDSS. These pixels appeared as dramatic spikes or dips in flux – we manually removed these points and linearly interpolated over the region for ease of visualization of the spectra. Before continuing our analysis, we translated the wavelengths of the spectra into the quasar rest frame using improved systemic redshifts from Shen et al. (2018). We adopt these redshift measurements for the remainder of this investigation. To remove the aforementioned sky contamination that was often present at the edges of the spectra, we cropped them to cover roughly the wavelength regions spanning 1200–2600 Å in the quasar rest frame.

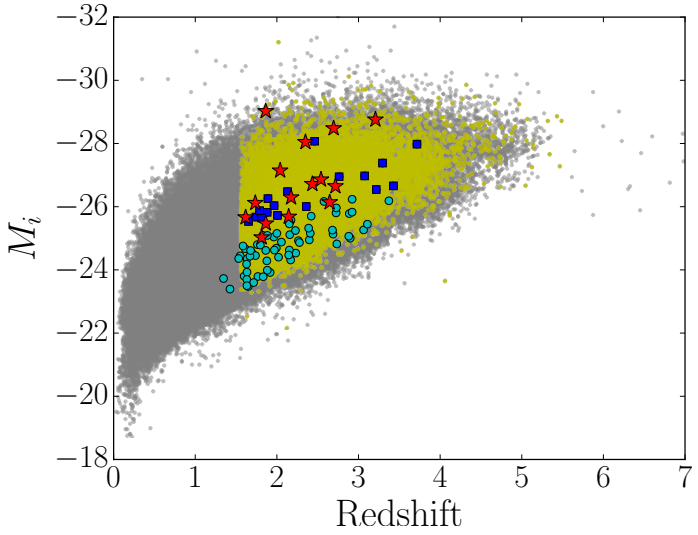

Figure 2.1 – Absolute i-magnitude as a function of redshift. Gray and yellow points show non-BAL and C IV-BAL quasars from the DR14 quasar catalog (Pâris et al. 2018), respectively. Cyan circles represent quasars in our initial 94-object sample that were cut due to low SN; blue squares show the quasars in our final sample that exhibit no significant short-term (<10-day) variability, and red stars indicate our 15 quasars that display significant short-term variability. Data for the SDSS-RM quasars were retrieved from Shen et al. (2018). All absolute magnitudes have been corrected to $M_i[z = 2]$, following Richards et al. (2006).

During the course of our study, we identified an issue with the SDSS pipeline reduction affecting data that were reduced after 2014. The issue was determined to be a result of incorrect background estimation in the presence of nearby standard stars during the extraction phase of the reduction process. Our team identified the affected fibers, if any, at each epoch in our sample and removed these individual spectra from our sample to avoid introducing systematic uncertainties from this issue. Eighteen of the quasars in our sample had at least one epoch that was removed. For some of these quasars only a single epoch was affected (e.g., RM 770), while in others, all of the post-2014 epochs were removed from the sample (e.g., RM 786).

2.4 Magnitude & Signal-To-Noise Cuts

Because we are searching for small-amplitude BAL variability, we require our spectra to have reasonably high signal-to-noise ratios (SN) near the C IV region of the spectrum. To quantify the SN, we measure SN_{1700}, defined as the median of the SN of each pixel in the 1650–1750 Å region in the quasar rest frame. We follow previous work (e.g. Gibson et al. 2009a) and require our objects to have SN_{1700} of 6 or higher per pixel (SDSS spectra are binned to 69 km s^{-1} per pixel). To achieve this, we selected only quasars with i-band magnitudes $m_i < 20.4$, which mostly eliminated quasars with SN lower than this threshold (see Figure 2.2). This m_i constraint restricted the sample to 36 objects. Figure 2.2 displays m_i vs. the median SN_{1700} measured within all available epochs for each quasar.

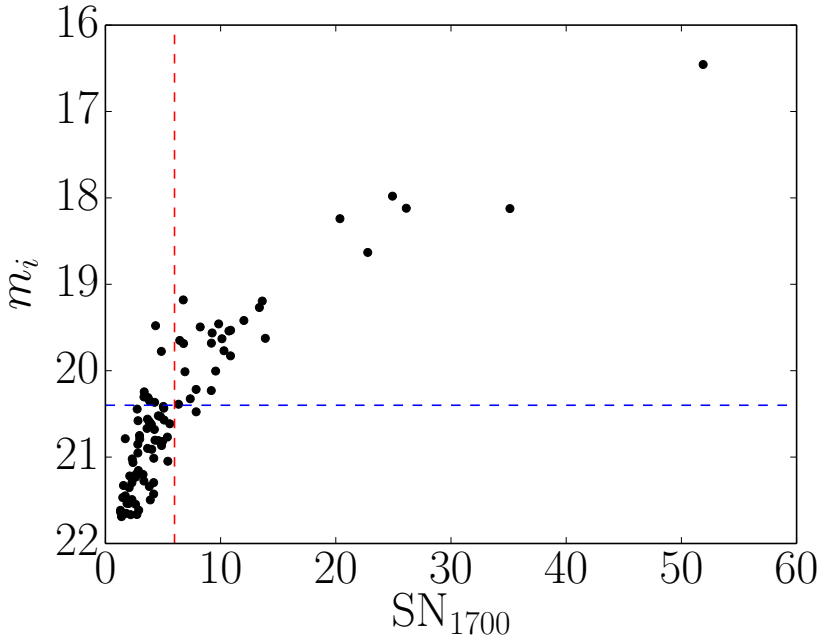

Figure 2.2 – The quasar apparent i-magnitude (m_i) vs. median SN_{1700} for the entire SDSS-RM BAL parent sample. The dashed blue line represents the location of our i-magnitude limit, and the dashed vertical red line shows the SN_{1700} cut. We note, however, that the SN_{1700} cut was made on individual spectral epochs, while the figure includes the median SN_{1700} of all spectra for each quasar.

Even after this magnitude cut, some individual epochs of some objects had a fairly low SN due to variations in observing conditions. Often, a reliable continuum fit was difficult to obtain for these epochs, rendering further measurements difficult or impossible. We impose a subsequent SN_{1700} cut of six on each individual spectral epoch to remove epochs where reliable fits were not feasible due to low SN. For some quasars, this action merely removed an epoch or two from our sample, while in four cases, all observations of the given quasar were dropped. There is some scatter in the relationship between m_i and SN_{1700}, and these four objects fell below our SN threshold despite our m_i cut; see Figure 2.2. Imposing this SN limit yielded 32 quasars that potentially host C IV BALs.

2.5 Continuum & Emission-Line Fitting

We follow previous BAL-variability studies (e.g. Filiz Ak et al., 2012, 2013; Grier et al., 2015, 2016) and use a least-squares fitting algorithm to fit reddened power laws to all spectra using the SMC-like reddening model of Pei (1992). We began the fitting process by adopting the relative line-free (RLF) regions determined by Gibson et al. (2009b), with a few revisions made after consulting the composite quasar spectra published by Vanden Berk et al. (2001) to identify regions relatively free of emission or absorption. Most quasars required additional deviations from the Gibson et al. (2009b) regions for optimal continuum fits due to the presence of strong absorption

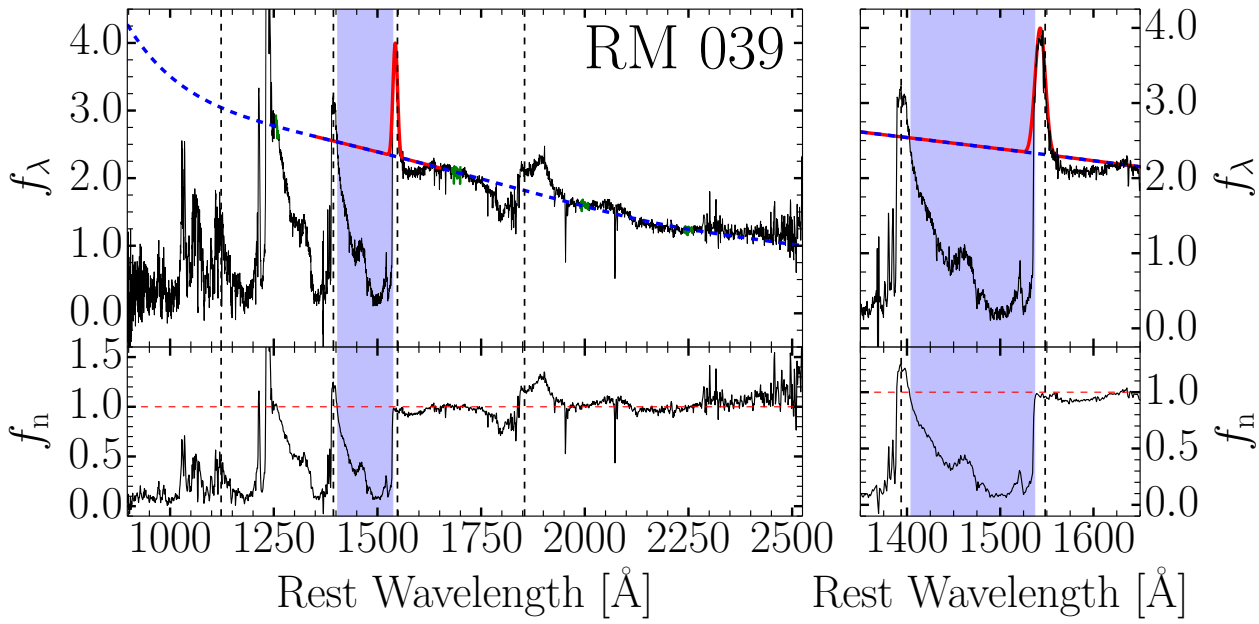

Figure 2.3 – The mean spectrum of quasar RM 039 using data from the first year of the SDSS-RM campaign (2014). The top subpanels show the quasar flux density, and the bottom subpanels show the continuum+emission-line-normalized fluxes f_n. The left panels show a large portion of the spectrum, while the right panels have zoomed in to show the C IV region. Thick dashed blue lines represent the continuum fits, solid red lines represent our C IV emission-line fits, and green regions show the adopted continuum regions used in the continuum fits. Shaded regions show the C IV BALs identified in each object. Blue shaded regions display the highest-velocity BAL in each spectrum, and red shaded regions display the lowest-velocity BAL. The horizontal red dashed lines in the bottom subpanels show a normalized flux of 1.0 to guide the eye. Vertical dotted lines indicate the rest-frame wavelengths of various species of interest: P V (1115 Å), Si IV (1393.8 Å), C IV (1548.2 Å), and Al III (1854.7 Å). Figures for all 27 quasars in our final sample are provided in a supplementary file.

or emission within the region. For a given quasar, we adopted the same RLF fit regions for all epochs. Because we manually adjusted the line-free regions, the iterative sigma-clipping techniques frequently employed in previous work (e.g., Filiz Ak et al. 2013) were not used. One epoch of one quasar (RM 284, MJD 57451) was missing sections of the spectrum toward the red end, causing difficulties with the continuum fits; we exclude this epoch from our analysis, as the missing pixels rendered a reasonable fit unobtainable.

For some spectra, the best-fit power law was consistent with no reddening, so we adopted a simple power law for our continuum — our choices of reddened or unreddened fits are indicated for each quasar in Table 3.1. Uncertainties in the continuum fits were determined using Monte Carlo methods; the flux values of each pixel within the fitting region were altered by a random Gaussian deviate scaled to the pixel uncertainties, and the spectra were subsequently refit. Our continuum fits to the mean spectra created from the 2014 observations are presented in Figure 2.3.

Several quasars exhibited BALs at velocities insufficient to cleanly separate them from the

C IV emission line. To remove the emission-line contamination from the BAL features, we follow Grier et al. (2015) and fit Gauss-Hermite (van der Marel & Franx, 1993), double-Gaussian (Park et al., 2013), and Voigt profile (Gibson et al., 2009b) models to the C IV emission line. To do this, we constructed mean spectra for each object for each individual year of the campaign. These mean spectra were assembled from all epochs passing our SN_{1700} threshold criterion defined in Section 2.4. For each object, we choose the best-fit model (Gauss-Hermite, double-Gaussian, or Voigt) based on visual inspection; the chosen models for each quasar are listed in Table 3.1. We adopt the fit parameters from the mean spectrum (except the amplitude parameter) for all epochs in a given year (i.e., the 2014 mean spectrum fit parameters were used for all 2014 SDSS-RM epochs, etc.). We then fit the emission lines to each individual epoch while allowing only the amplitude parameter to vary. This process assumes that only the amplitude of the emission lines varied within the same observing season and all other characteristics (e.g., widths, centers, etc) remained constant. Our emission-line fits are displayed in Figure 2.3. We add the continuum and emission-line fits together — these fits are hereafter referred to as the "continuum+emission-line" fits.

Chapter 3

Final Sample Selection & BAL Measurements

3.1 Final BAL Quasar Sample

We are primarily interested in quasars that host C IV BALs at the beginning of the campaign. To search for such BALs, we first binned all of the 2014 mean normalized spectra by three pixels to account for SDSS oversampling of the spectral line function. Binning ensures that neighboring pixels are almost entirely uncorrelated. We then smoothed the binned spectra by three pixels. We note that smoothing was used only for the BAL search to reduce noise; we make all additional measurements on the un-smoothed (but binned) spectra. We then searched each of the 2014 mean spectra for regions in which the normalized flux density drops below 0.9 for velocity widths greater than 2000 km s^{-1} (i.e., a BAL exists that is consistent with the formal definition of Weymann et al. 1991). We restricted our search to within 30,000 km s^{-1} blueward of the C IV rest wavelength and include BALs that extend redward of C IV out to 1000 km s^{-1}. Quasars without formal C IV BALs in their 2014 mean spectra, such as those containing only mini-BALs or those for which a BAL did not appear until later on in the campaign, were dropped from our sample.

After identifying the BALs, we visually inspected all spectra to ensure that the BALs were not contaminated by residual sky flux or bad pixels. Three BALs were found to either have bad pixels within the BAL trough (RM 528 and RM 729) or to contain residual sky lines within the BAL (RM 195) that could potentially affect our analysis. These BALs were excluded from our sample. Resultantly, RM 528 was removed from our sample, as there was only one BAL present in this quasar. The two other aforementioned quasars had remaining uncontaminated BALs present in the spectrum, and so remain in our final sample.

The final sample contains 27 quasars with 37 uncontaminated C IV BALs between them. We present basic information on our final sample of BAL quasars in Table 3.1 and provide information on each individual identified BAL in Table 3.2. To distinguish between C IV BALs when more than one is present in a spectrum, we assign identifiers [A] and [B] to the BALs as wavelength increases (and as the velocity decreases); therefore, in cases with multiple BALs, [A] refers to the higher-velocity BAL, and [B] to the lower-velocity BAL (none of our quasars contained more than two C IV BALs). The regions of the spectra containing the C IV BALs in each quasar are highlighted in Figure 2.3. Our final sample of BAL quasars does not generally have properties different from those of the larger BAL-quasar population (see Figure 2.1). Most (26 out of 27) of the quasars in our sample are radio quiet and are undetected by the FIRST radio survey (White et al. 1997; compiled by Shen et al. 2018). The one exception is RM 155, which has a measured radio-loudness parameter of $R = 42.89$. R is defined as the ratio of fluxes at 6 cm and 2500 Å (e.g., Shen et al. 2018).

Our final sample of spectra has a median of 58 epochs per object; this is the highest of any BAL variability study by almost a factor of 10 (see Table 1.1). Figure 3.1 displays the distribution of rest-frame time difference between all pairs of subsequent epochs (hereafter referred to as $\Delta t_{\rm rest}$) for the sample, including only sequential pairs of epochs for each quasar that are separated by less than 10 days in the quasar rest frame. Hereafter, we refer to all variability on timescales of less than 10 days in the quasar rest frame as "short-timescale", or "rapid" variability. Epochs separated by rest-frame timescales on the order of a single day are frequent. The median rest-frame time resolution of the SDSS-RM observations among our sample of quasars is 2.4 days, nearly a factor of 10 lower than even the shortest-timescale studies previously reported (see Table 1.1). Our sample spans a redshift range of 1.62 to 3.72, which is comparable to previous studies (this is by

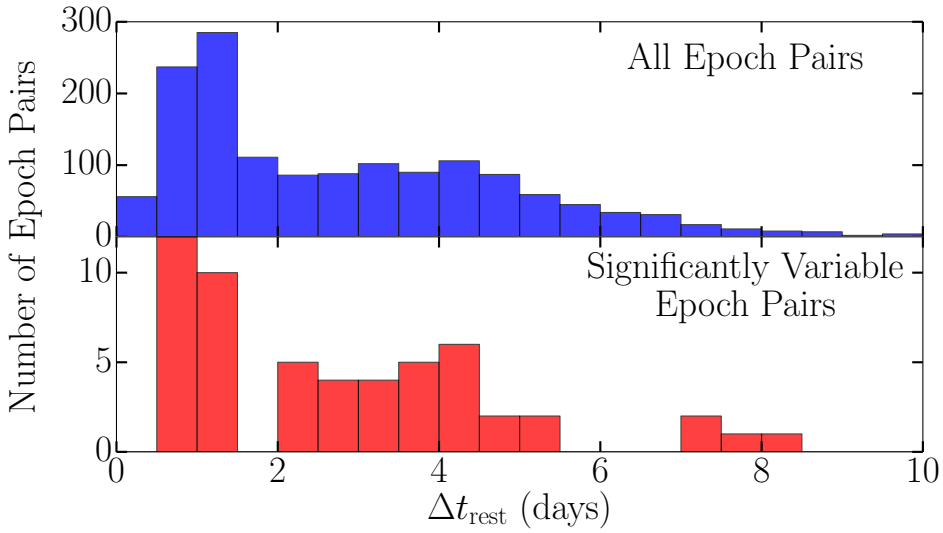

Figure 3.1 – Histogram of the rest-frame time difference $\Delta t_{\rm rest}$ distribution of our sample. The top panel shows a histogram for our entire 27-object sample; the bottom panel uses only those pairs of epochs showing significant short-timescale variability (see Section 3.3). The region $\Delta t_{\rm rest} < 2$ days is well-populated.

necessity, as the the C IV region must be redshifted to within the range of spectral coverage of the instruments used in each study).

3.2 Additional BAL Measurements

After identifying the BALs and creating our final sample, we determined the BAL velocity bounds ($v_{\rm min}$ and $v_{\rm max}$) for each BAL feature from the pixels for which the normalized flux density recovered to 0.9 or higher at either end of the trough. Although the BALs are blueshifted relative to the emission lines, we here define our velocity ranges as positive-increasing in the shorter-wavelength direction. We calculated the rest-frame equivalent widths (EWs) for each BAL, along with rest-frame mean fractional depth $\langle d \rangle$ and absorbed-flux weighted centroid velocity ($v_{\rm cent}$). The EW and $v_{\rm cent}$ are defined as follows:

$$\mathrm{EW} = \int_{\lambda_{\rm min}}^{\lambda_{\rm max}} [1 - \mathrm{f_n}(\lambda)]\, \mathrm{d}\lambda \tag{3.1}$$

$$v_{\rm cent} = \frac{\int_{v_{\rm min}}^{v_{\rm max}} v[1 - f_n(v)]\, dv}{\mathrm{EW}} \tag{3.2}$$

where f_n is the continuum-normalized flux across the BAL trough. We propagate the normalized spectral uncertainties to determine the uncertainty in our EW measurements. We provide these measurements from the 2014 mean spectra for our final sample in Table 3.2. The EW measurements of each BAL as a function of the Modified Julian Date (MJD) for each quasar are presented

Table 3.1. Final Quasar Sample Information

SDSS ID	RM ID	RA[a] (deg)	DEC[a] (deg)	z[a]	m_i[a]	SN (1700)	N (epochs)	$\Delta t_{\rm rest}$ (days)	Con Fit[b]	Line Fit[c]
J141607.12+531904.8	RM 039	214.02967	53.31800	3.08	19.77	10.24	58	2.88	R	V
J141741.72+530519.0	RM 073	214.42385	53.08863	3.43	20.37	6.76	3	7.34	R	DG
J141432.46+523154.5	RM 116	213.63526	52.53182	1.88	19.68	9.50	64	3.99	R	DG
J141103.17+531551.3	RM 128	212.76324	53.26426	1.86	20.01	7.25	50	3.60	R	V
J141123.68+532845.7	RM 155	212.84871	53.47936	1.65	19.65	7.14	41	2.61	R	DG
J141935.58+525710.7	RM 195	214.89825	52.95297	3.22	20.33	7.66	59	2.75	R	DG
J141000.68+532156.1	RM 217	212.50287	53.36560	1.81	20.39	7.12	41	2.46	R	V
J140931.90+532302.2	RM 257	212.38295	53.38395	2.43	19.54	10.88	65	3.02	U	V
J141927.35+533727.7	RM 284	214.86398	53.62436	2.36	20.22	8.16	63	3.46	U	GH
J142014.84+533609.0	RM 339	215.06184	53.60252	2.01	20.00	9.68	64	3.47	R	DG
J141955.27+522741.1	RM 357	214.98029	52.46144	2.14	20.23	9.25	65	3.49	R	DG
J142100.22+524342.3	RM 361	215.25092	52.72844	1.62	19.46	9.92	66	3.94	R	V
J141409.85+520137.2	RM 408	213.54107	52.02702	1.74	19.63	10.27	65	4.00	R	DG
J142129.40+522752.0	RM 508	215.37253	52.46445	3.21	18.12	35.09	69	2.21	R	DG
J142233.74+525219.8	RM 509	215.64060	52.87219	2.65	20.30	6.51	10	3.84	R	V
J142306.05+531529.0	RM 564	215.77521	53.25807	2.46	18.24	20.36	67	2.69	U	DG
J140634.14+525407.8	RM 565	211.64227	52.90219	1.79	19.48	6.25	3	13.78	U	V
J141007.73+541203.4	RM 613	212.53224	54.20095	2.35	18.12	26.18	68	2.87	R	V
J140554.87+530323.5	RM 631	211.47865	53.05655	2.72	19.83	11.28	65	2.79	R	GH
J141648.26+542900.9	RM 717	214.20109	54.48360	2.17	19.69	7.18	49	3.74	R	DG
J142419.18+531750.6	RM 722	216.07996	53.29739	2.54	19.49	8.65	59	3.10	U	DG
J142404.67+532949.3	RM 729	216.01946	53.49704	2.76	19.56	9.66	63	2.91	R	V
J142225.03+535901.7	RM 730	215.60432	53.98381	2.69	17.98	24.74	65	2.81	R	GH
J142405.10+533206.3	RM 743	216.02126	53.53509	1.74	19.18	6.97	49	3.47	R	DG
J142106.86+533745.2	RM 770	215.27862	53.62923	1.86	16.46	51.89	69	3.25	R	DG
J141322.43+523249.7	RM 785	213.34349	52.54715	3.72	19.19	13.81	67	2.11	U	GH
J141421.53+522940.1	RM 786	213.58974	52.49447	2.04	18.63	22.96	68	3.17	R	None

[a]J2000 Position, redshift, and magnitude measurements were obtained from SDSS Data Release 10 (Ahn et al. 2014). The i-magnitudes provided above are point-spread function magnitudes that have not been corrected for Galactic extinction.

[b]A designation of "R" indicates that a reddened power law continuum fit was used for this quasar, and a designation of "U" indicates the use of an unreddened power law.

[c]A designation of "V" indicates that a Voigt profile to was used to represent the C IV emission line, "DG" indicates the use of a double-Gaussian profile, "GH" indicates a Gauss-Hermite profile was used, and "None" indicates that we were unable to obtain any acceptable emission-line fit, so the continuum-only fit was adopted.

Table 3.2. 2014 Mean Spectra CIV BAL Measurements

RM ID	BAL ID	v_{max}[a]	v_{min}[a]	v_{cent}[a]	$\langle d \rangle$	EW (Å)	FA14 ID[b]	PV
RM 039	A	29148	2190	13445	0.67	88.5±0.7	CIV_{SA}	Y
RM 073	A	10142	5768	7821	0.23	5.1±0.4	CIV_{00}	N
RM 073	B	4586	1456	2680	0.51	8.0±0.2	CIV_{00}	N
RM 116	A	11599	5467	7946	0.26	8.2±0.3	CIV_{S0}	···
RM 116	B	4860	2746	3650	0.36	4.0±0.2	CIV_{00}	···
RM 128	A	21360	4814	10569	0.38	31.5±0.7	CIV_{S0}	···
RM 128	B	2691	583	1486	0.22	2.5±0.2	CIV_{00}	···
RM 155	A	7670	447	3249	0.54	19.9±0.4	CIV_{SA}	···
RM 195	A	3243	378	1788	0.41	5.9±0.1	CIV_{00}	N
RM 217	A	19323	14820	17014	0.19	4.2±0.4	CIV_{S0}	···
RM 217	B	11640	2901	6379	0.47	20.8±0.5	CIV_{S0}	···
RM 257	A	24762	6659	13586	0.48	42.6±0.4	CIV_{SA}	Y
RM 257	B	4117	2098	3067	0.50	5.2±0.1	CIV_{00}	N
RM 284	A	24141	19496	21736	0.12	2.8±0.2	CIV_{N0}	···
RM 339	A	15188	7789	10850	0.26	9.7±0.3	CIV_{SA}	···
RM 357	A	14782	11935	13284	0.15	2.2±0.3	CIV_{00}	···
RM 357	B	7152	1891	3934	0.53	14.1±0.3	CIV_{S0}	···
RM 361	A	7122	1463	3980	0.54	15.3±0.3	CIV_{N0}	···
RM 408	A	4451	656	2201	0.50	9.8±0.2	CIV_{00}	···
RM 508	A	21344	18101	19590	0.36	5.7±0.1	CIV_{00}	N
RM 509	A	24553	13814	18176	0.26	13.6±0.5	CIV_{S0}	N
RM 509	B	2464	337	1371	0.46	5.1±0.1	CIV_{00}	N
RM 564	A	25282	21819	23559	0.17	2.8±0.1	CIV_{S0}	···
RM 565	A	27794	14010	20647	0.21	13.7±1.3	CIV_{N0}	···
RM 565	B	13688	3878	8127	0.24	11.7±1.0	CIV_{S0}	···
RM 613	A	20046	15713	17872	0.22	4.8±0.2	CIV_{00}	···
RM 631	A	8931	5858	7295	0.47	7.2±0.2	CIV_{S0}	Y
RM 717	A	23343	8567	15064	0.30	21.8±0.7	CIV_{S0}	···
RM 722	A	6238	2063	3955	0.58	12.5±0.2	CIV_{00}	N
RM 729	A	9754	3465	6306	0.37	11.8±0.3	CIV_{S0}	Y
RM 730	A	27969	15310	22035	0.40	24.5±0.2	CIV_{S0}	Y
RM 730	B	14823	11675	12893	0.15	2.5±0.1	CIV_{00}	N
RM 743	A	11177	4423	7402	0.31	10.6±0.6	CIV_{SA}	···
RM 770	A	20663	15904	18231	0.15	3.6±0.1	CIV_{00}	···
RM 785	A	26858	12732	19713	0.21	14.3±0.3	CIV_{S0}	Y
RM 786	A	14967	11437	13062	0.15	2.7±0.2	CIV_{00}	···
RM 786	B	8814	-338	3456	0.75	34.4±0.2	CIV_{SA}	···

[a]Velocities are in units of km s^{-1}.

[b]BAL designation according to whether or not BALs or mini-BALs are present for Si IV and Al III, as defined by Filiz Ak et al. (2014); see Section 4.3.3. A designation of CIV_{N0} indicates that the Si IV line is not completely covered by our spectrum at those velocities or we are unable to otherwise determine whether or not it is present, so we are unsure of the designation.

[c]This column indicates whether or not there is a suspected corresponding PV BAL or mini-BAL (see Section 4.3.3): "Y" indicates that PV is present; "N" indicates that it is not. Entries with no data indicate that the PV region is not covered by the SDSS spectra.

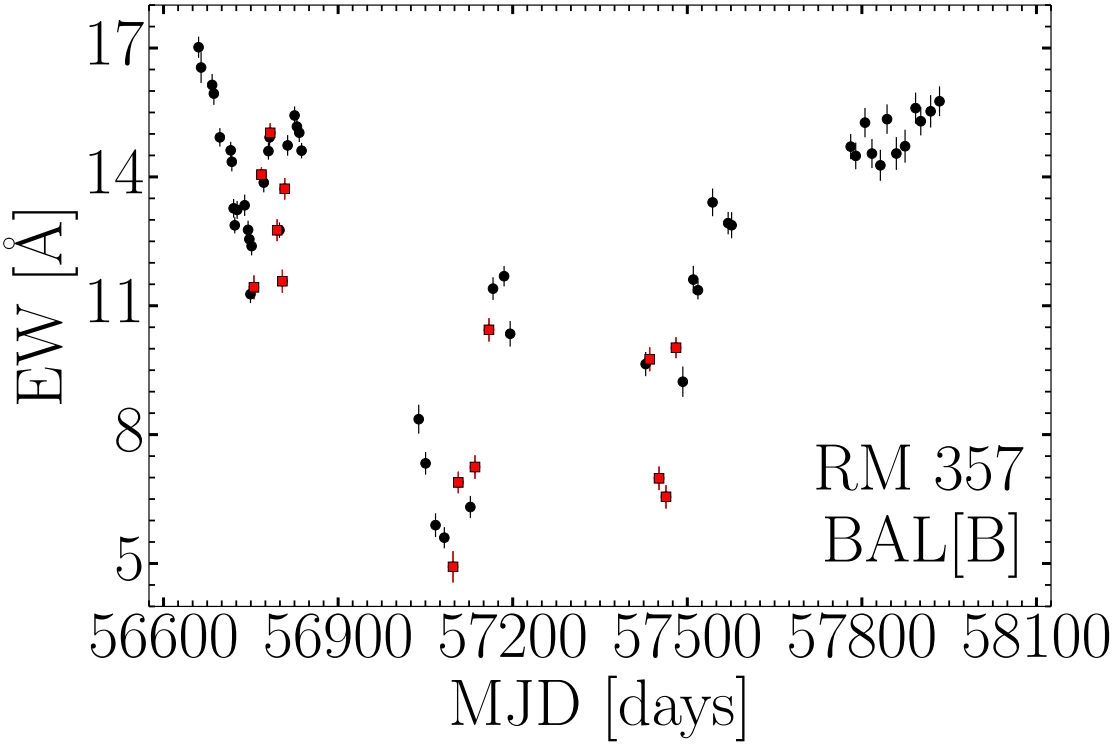

Figure 3.2 – EW v. MJD for RM 357 BAL[B]. Epoch pairs that satisfy our criteria for significant short-term variability (see Section 3.3) are marked by red squares. Figures for all 37 individual BALs in our sample are provided in the online version of the article.

in Figure 3.2. Nearly all of our BALs show significant variability across the four years of monitoring — most of the EW light curves reveal visible trends across even a single observing season.

3.3 Detection of Significant Variability

We began our investigation by measuring ΔEW, the change in equivalent width of the BAL between two subsequent epochs. We calculated the uncertainty in the ΔEW parameter using a basic quadrature sum of the uncertainties in the equivalent widths for each epoch of interest. As discussed above, we did remove some epochs from our sample due to various issues (low SN, bad sky subtraction, etc); therefore the cadence varies from object to object from the original SDSS-RM cadence. Figure 3.3 shows the distribution of ΔEW for all sequential pairs of epochs for our sample. The distribution of ΔEW is centered on zero and contains mostly small-amplitude variations, though there are rare cases of more dramatic variability, particularly on timescales ranging from 10-100 days in the quasar rest frame.

To identify significant variability between pairs of epochs, we follow previous works and re-

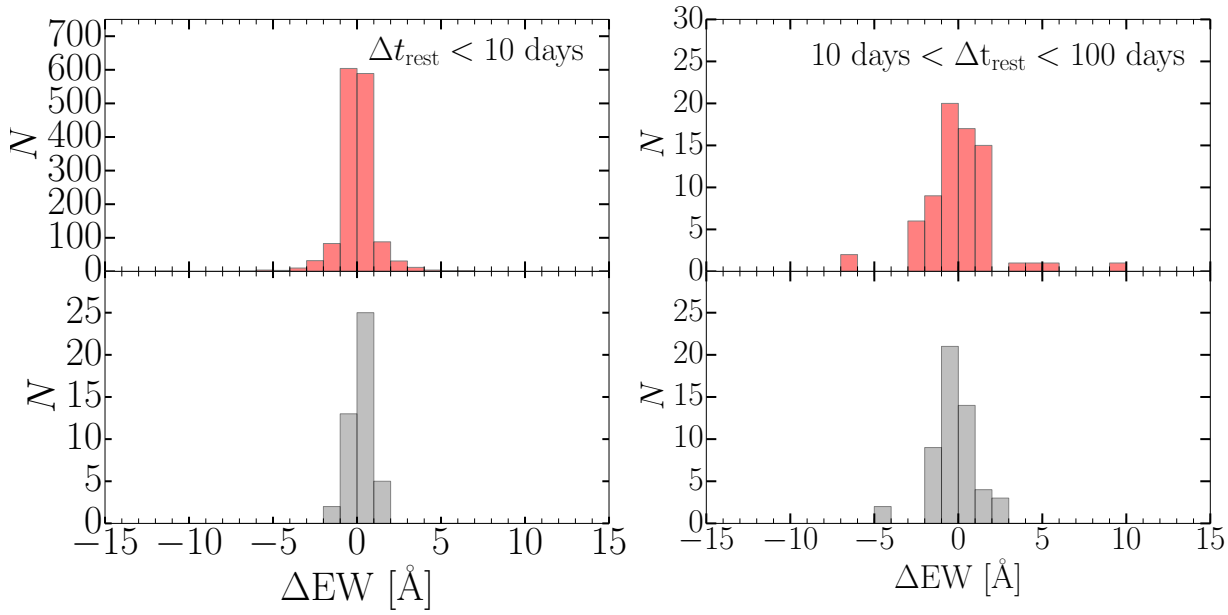

Figure 3.3 The distribution of ΔEW among BAL quasars. Panels with red histograms show measurements from our work using all pairs of sequential epochs for each quasar in our sample. Panels with gray histograms represent data from Barlow (1993), Lundgren et al. (2007), Gibson et al. (2008), and Filiz Ak et al. (2013). The top two panels show the distributions for epochs that are separated by 0–10 days in the quasar rest frame and the bottom two panels show the distributions for epochs separated by 10–100 days in the quasar rest frame. See Section 4.2 for a comparison between our work and previous studies.

quire that the ratio of ΔEW to its uncertainty, $\sigma_{\Delta\mathrm{EW}}$, be at least four (i.e., we impose a 4σ significance requirement on ΔEW). However, solely using the aforementioned significance criteria returned several seemingly false-positive cases of short-term variability, as in several cases nearby regions outside the BAL also displayed considerable variability. This behavior suggests that the variability observed within the BAL may be due to inconsistencies in continuum fits or overall spectral variability not associated with the BAL itself. These inconsistencies are probably due to nearby emission-line variability or a lack of line-free regions close to the BAL, which, combined with noise, causes the continuum fits to vary somewhat from epoch to epoch. Such cases motivated the use of additional criteria which could isolate true BAL variability from variations in continuum and emission-line fits. To address this issue, we define a quantity hereafter referred to as G:

$$G = \frac{\chi^2 - (N-1)}{\sqrt{2(N-1)}} \tag{3.3}$$

where the χ^2 quantity is the the square of the difference between the fluxes at two spectral epochs divided by their average uncertainty, summed over the N pixels within a specified region. The expected value and standard deviation of the distribution of the χ^2 statistic for a region of N pixels are $N-1$ and $\sqrt{2(N-1)}$, respectively; thus the G statistic should have a mean of 0 and standard deviation of 1 if there are no variations between the two spectra. Higher values of G indicate inconsistencies between the two spectra (indicating variability) at various levels of significance.

For each BAL, we located nearby regions that contained very few features, hereafter referred to as "continuum" regions. Because we did not fit the nearby Si IV emission line, this region (and all regions blueward) were not included in the continuum regions. Continuum regions redward of Si IV were selected via visual inspection, referencing the composite quasar spectra of Vanden Berk et al. (2001) to search for wavelength regions with minimal contaminants. We then determined the G values in the identified continuum regions as well as within the BAL region. Hereafter, we refer to these G values as G_{C} and G_{B}, respectively.

We are searching for cases where there is variability in the normalized spectra within the BAL region but *not* within the continuum regions. For a pair of spectra to be considered to show "significant" variability, we require that $G_{\mathrm{B}} > 4$ and $G_{\mathrm{C}} < 2$. Figure 3.4 demonstrates the use of these criteria in excluding cases of spurious detections from our sample. It is possible that these criteria will exclude cases of true BAL variability due to random fluctuations in the continuum regions; however, the use of these criteria allows us to create a more clean and conservative sample of spectra showing significant short-timescale BAL variability.

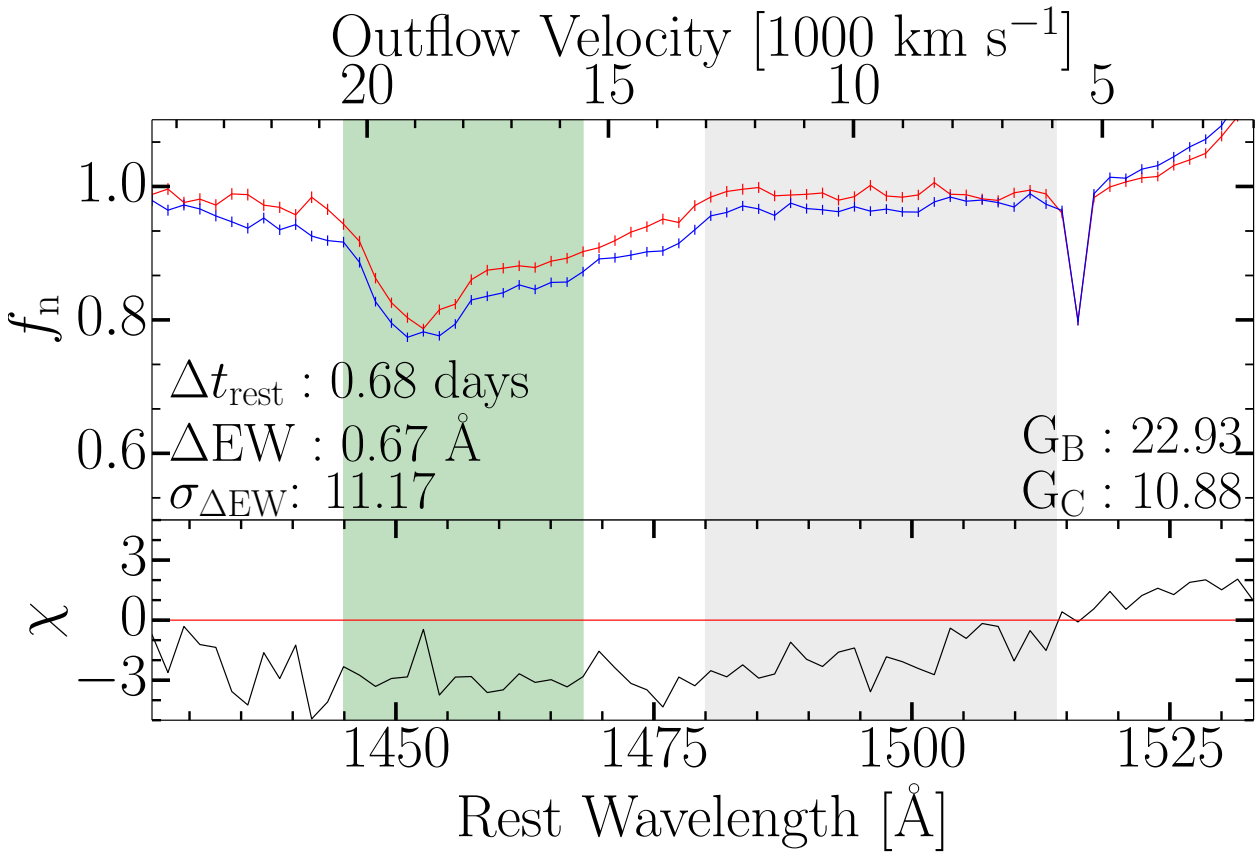

Figure 3.4 A demonstration of the utility of our additional significance criteria. The spectra shown are from RM 770, MJDs 56715–56717. The top subpanel shows the normalized flux, f_n. The red line and error bars correspond to the first epoch listed, and blue corresponds to the second epoch. The gray shaded region displays the continuum region used to calculate G_C. The green shaded region highlights the region containing the BAL being examined — this region was used to calculate $G_{\rm B}$. Relevant measurements ($\Delta t_{\rm rest}$, ΔEW, $\sigma_{\Delta \rm EW}$, $G_{\rm B}$, and $G_{\rm C}$) are provided. The bottom subpanel shows the χ statistic (showing the difference between the two spectra in units of their uncertainties) as a function of wavelength.

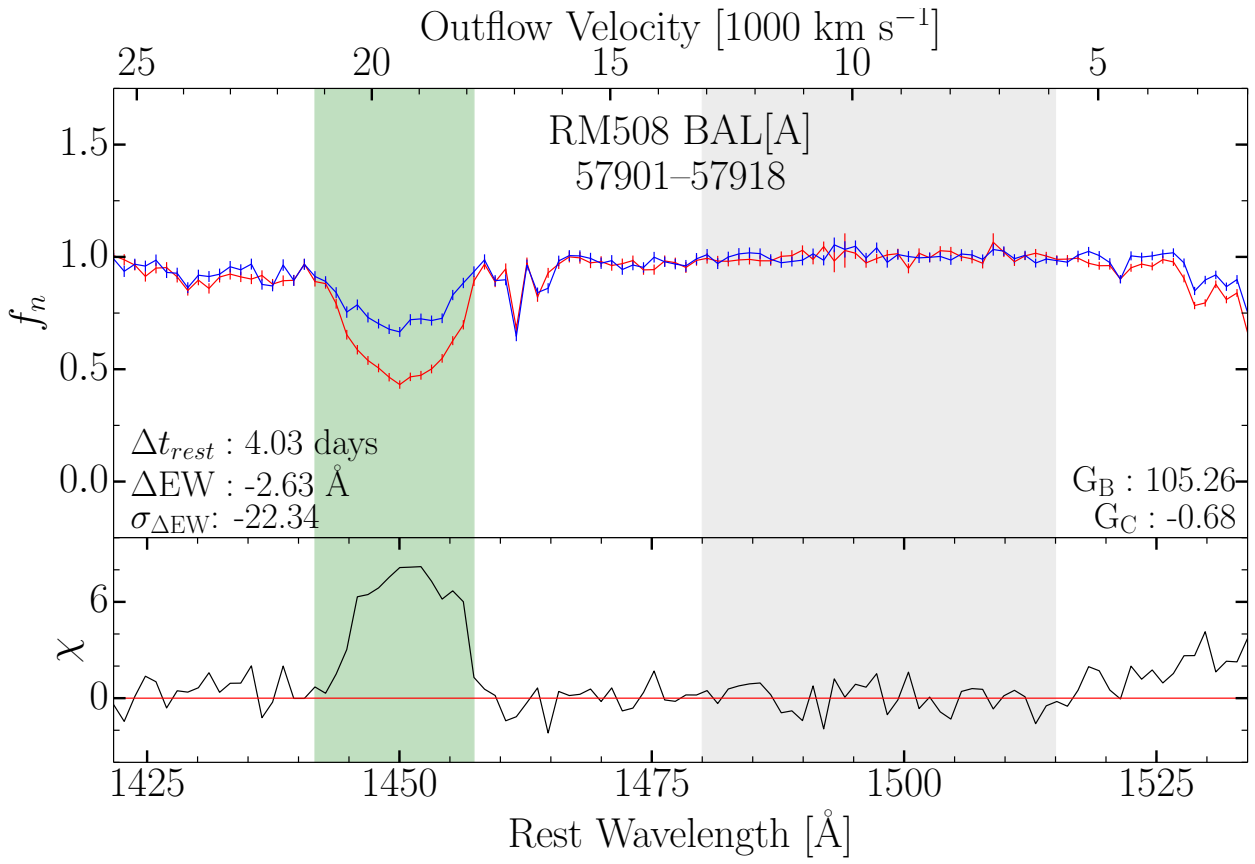

Figure 3.5 Pairs of spectra showing "significant" variability for one pair of epochs for RM 508. The top subpanels show the normalized flux, f_n, with the MJDs of the two epochs provided below the RM identifier in the title of each plot. The red line and error bars correspond to the first epoch listed, and blue corresponds to the second epoch. The gray shaded regions display the continuum regions used to calculate G_C. The green shaded region highlights the region containing the BAL being examined — this region was used to calculate G_B. Yellow shaded regions indicate additional C IV BALs, when present. Relevant measurements ($\Delta t_{\rm rest}$, ΔEW, $\sigma_{\Delta EW}$, G_B, and G_C) are provided for each pair of spectra. The bottom subpanels for each pair show the χ statistic (showing the difference between the two spectra in units of their uncertainties) as a function of wavelength. Figures for all 54 instances of significant short-timescale variability are provided in a supplementary file.

Chapter 4

Results & Discussion

4.1 BALs Exhibiting Short-Timescale Variability

We searched for short-timescale variability in our sample by identifying pairs of epochs with significant variability (as defined above) on rest-frame timescales of less than 10 days. Figure 3.5 shows all pairs of spectra in which we identified significant short-timescale variability and Table 4.1 provides information on which epochs show significant variability as well as the relevant measurements. We identify 54 epoch pairs in 19 unique BALs in 15 different quasars that show significant variability on these short timescales (four quasars had two C IV BALs present that both varied significantly). This suggests that short-timescale BAL variability occurs in at least $55^{+18}_{-14}\%$ of BAL quasars (upper and lower confidence limits, here and henceforth, are all calculated via Gehrels 1986, unless noted otherwise). This frequency is significantly higher than that reported by Capellupo et al. (2013); they found that only $12^{+15}_{-7.6}\%$ (two quasars in their sample) showed significant variability on timescales of less than 72 days (they report 29% for a less-conservative estimate). We also examine the frequency of rapid variability in each epoch. We have a total 1460 pairs of sequential epochs in our sample. Out of these 1460 pairs, we find that 54 ($3.7 \pm 2.6\%$ of all epoch pairs) exhibit significant short-timescale variability.

We examined several properties of the 15 quasars exhibiting significant short-term variability (M_i, z, radio-loudness) and find that none of them is an outlier compared to the general population of BAL quasars (see Figure 2.1) and none of them are radio-loud. Additionally, we investigated whether the BAL troughs that exhibit significant short-timescale variability are distinct from BAL troughs that do not exhibit such variability in terms of velocity width, mean depth, EW, and centroid velocity (Δv, $\langle d \rangle$, EW, and $v_{\rm cent}$). The parameter distributions of the varying and non-varying BALs were compared using a two-sample Kolmogorov-Smirnov (K-S) test, returning the K-S statistic (D) and the corresponding probability P, which represents the probability that the two samples are drawn from the same parent distribution. We measure D = 0.17 and P = 0.94 for Δv, D = 0.17 and P = 0.94 for $\langle d \rangle$, D = 0.21 and P = 0.80 for EW, and D = 0.22 and P = 0.72 for $v_{\rm cent}$. Thus, we conclude that varying and non-varying BALs do not fundamentally differ in terms of the aforementioned parameters.

In this sample, we find significant variability on timescales down to 0.57 days, nearly as short as our data probe (the shortest rest-frame timescale probed for each object ranges between 0.1 and 0.3 days, depending on their redshifts). This is the first detection of such short-term variability, to our knowledge, likely because our study intensively probes timescales much shorter than previous works (see Table 1.1). BAL variability has thus far been observed on all timescales that have been examined.

A variety of variability amplitudes appear in our rapidly-varying pairs of spectra; however, in most cases, the fractional change in EW is fairly small (this is expected, as previous studies have established that the fractional change in EW increases with timescale). We do not see a preference for variability in either the positive or negative direction — i.e., the BAL troughs do not preferentially weaken or strengthen on these short timescales (26 out of 54 epoch pairs show a decrease in EW, while 28 out of 54 epoch pairs show an increase in EW).

In some cases, however, rather dramatic variability occurs. For example, toward the end of the 2017 observations (MJD 57901 to 57918), we observe a dramatic change in the BAL in RM 508; the EW dropped from 6.12 Å to 3.49 Å (a factor of 1.8) within a time span of about 4 days in the quasar rest frame (see Figure 3.5).

Another example of more dramatic variability is RM 357, which has a high-velocity BAL (denoted BAL[A] in our tables and figures) that is present at the beginning of the campaign but disappears and reappears at various points during the campaign.

The absorption in the region containing BAL[A] had steadily weakened during the first few months of the campaign (see Figure 3.2), its EW decreasing to within 3σ of zero by MJD 56755 (it is no longer formally considered a BAL at this point). The absorption feature then reappeared as a formal BAL between MJD 56755 and 56768 ($\Delta t_{\rm rest} = 4.1$ days), and disappeared again between MJD 56783 and 56795 ($\Delta t_{\rm rest}$ = 3.79 days). In both epochs where the BAL is not present (MJDs 56755 and 56795), we searched for residual low-level absorption. We consider there to be no residual absorption if all pixels within the trough region deviate by less than 3σ from the continuum flux. We see no residual absorption at this level in both of these epochs — we thus consider these to be "pristine" cases of BAL disappearance (see, e.g., Filiz Ak et al. 2012 or De Cicco et al. 2018 for further examples of "pristine" BAL disappearance).

4.2 Variability Characteristics of the Entire Quasar Sample

We now compare the distributions of some variability parameters within our sample with those from previous studies to determine how they fit within the context of previous results.

Figure 3.3 shows the distribution of ΔEW in every sequential pair of epochs for our entire quasar sample compared with previous work, Figure 4.1 displays ΔEW as a function of $\langle$EW$\rangle$, and Figure 4.2 shows the distribution of ΔEW and ΔEW$/\langle$EW$\rangle$ as a function of time. There were two BALs that disappeared at some point during the campaign (RM 217 BAL[A] and RM 357 BAL[A]); in cases where these BALs were absent in two sequential epochs, our EW and ΔEW measurements measure primarily just spectral noise, as there is no BAL present. For our sample investigations (Figures 4.1 and 4.2), we thus exclude pairs of epochs in all quasars where both of the EW values are consistent with zero to within 3σ.

These three figures together reveal that there are no significant outliers in ΔEW (either as a function of $\langle$EW$\rangle$ or with Δt$_{\rm rest}$) within our sample compared to the distribution found by previous studies. We do see some epoch pairs that appear to show more variability than expected at short timescales in Figure 4.2; however, as Figure 3.3 demonstrates, the majority of our measurements are small-amplitude variations, and these more extreme cases represent the tails of the distribution of ΔEW.

Table 4.1. Short-Timescale Variability Among Epoch Pairs

RM ID	BAL ID	MJD_1 (days)	MJD_2 (days)	Δt_{rest} (days)	EW_1 (Å)	EW_2 (Å)	$\Delta\mathrm{EW}$ (Å)	σ ($_{\Delta\mathrm{EW}}$)	G_{B}	G_{C}	f (>1)	f (<−1)	$\Delta \mathrm{v}_{\mathrm{co}}$ *
128	A	56768.23	56772.23	1.40	34.9 ± 0.5	31.6 ± 0.5	-3.3 ± 0.8	-4.26	5.15	-0.70	0.32	0.08	620
128	A	56783.25	56795.18	4.16	31.7 ± 0.7	26.4 ± 0.7	-5.3 ± 1.0	-5.08	4.46	0.39	0.32	0.09	610
128	B	56720.45	56722.39	0.68	1.7 ± 0.1	2.6 ± 0.1	0.9 ± 0.2	5.23	8.87	0.29	0.00	0.57	900
128	B	56825.19	56829.21	1.41	2.0 ± 0.1	3.1 ± 0.1	1.1 ± 0.2	5.50	9.41	1.29	0.00	0.86	1500
217	B	56660.21	56683.48	8.27	15.7 ± 0.5	19.2 ± 0.5	3.5 ± 0.7	4.93	4.13	-1.27	0.00	0.41	310
217	B	56683.48	56686.47	1.06	19.2 ± 0.5	16.3 ± 0.5	-2.9 ± 0.7	-4.30	4.33	0.28	0.56	0.15	940
217	B	56686.47	56696.78	3.66	16.3 ± 0.5	19.3 ± 0.4	3.1 ± 0.6	4.76	4.70	-0.77	0.07	0.48	630
257	A	57510.32	57518.31	2.33	40.6 ± 0.4	47.1 ± 0.5	6.4 ± 0.6	10.10	27.03	0.38	0.13	0.54	7250
257	A	57518.31	57543.45	7.32	47.1 ± 0.5	42.1 ± 0.5	-4.9 ± 0.7	-7.11	9.46	1.13	0.49	0.06	3650
257	B	56715.39	56717.33	0.57	4.9 ± 0.1	5.3 ± 0.1	0.4 ± 0.1	4.60	5.26	-0.66	0.00	0.75	510
257	B	56717.33	56720.45	0.91	5.3 ± 0.1	4.9 ± 0.1	-0.4 ± 0.1	-4.64	6.24	-0.42	0.75	0.00	510
257	B	57510.32	57518.31	2.33	4.9 ± 0.1	5.6 ± 0.1	0.7 ± 0.1	5.90	14.09	0.38	0.12	0.62	1010
257	B	57518.31	57543.45	7.32	5.6 ± 0.1	5.1 ± 0.1	-0.6 ± 0.1	-4.32	5.41	1.13	0.62	0.00	760
257	B	57918.16	57933.42	4.44	4.6 ± 0.1	5.3 ± 0.1	0.6 ± 0.1	5.06	7.20	-0.40	0.00	0.75	1010
357	A	56755.34	56768.23	4.10	0.6 ± 0.2	2.1 ± 0.2	1.5 ± 0.3	5.09	5.98	-0.80	0.00	0.80	1140
357	A	56783.25	56795.18	3.79	2.5 ± 0.2	0.6 ± 0.2	-1.9 ± 0.3	-6.08	8.68	1.59	0.90	0.00	2280
357	B	56755.34	56768.23	4.10	11.4 ± 0.3	14.1 ± 0.2	2.6 ± 0.3	8.07	17.98	-0.80	0.11	0.53	2220
357	B	56783.25	56795.18	3.79	15.0 ± 0.2	12.8 ± 0.3	-2.3 ± 0.3	-6.69	10.46	1.59	0.63	0.11	1950
357	B	56804.19	56808.26	1.29	11.6 ± 0.3	13.7 ± 0.2	2.2 ± 0.4	5.88	10.66	0.31	0.05	0.47	1110
357	B	57097.48	57106.47	2.86	4.9 ± 0.4	6.9 ± 0.3	2.0 ± 0.4	4.45	4.21	-0.98	0.00	0.53	550
357	B	57135.17	57159.16	7.63	7.2 ± 0.3	10.4 ± 0.3	3.2 ± 0.4	8.30	16.19	-1.33	0.00	0.68	1380
357	B	57435.40	57451.46	5.11	9.8 ± 0.3	7.0 ± 0.3	-2.8 ± 0.4	-7.10	15.12	0.48	0.68	0.05	1390
357	B	57463.40	57480.60	5.47	6.6 ± 0.3	10.0 ± 0.2	3.5 ± 0.4	9.49	19.82	1.89	0.00	0.79	2490
361	A	56813.23	56825.19	4.57	14.5 ± 0.2	16.7 ± 0.2	2.2 ± 0.3	6.29	7.54	1.80	0.00	0.65	2010
508	A	56686.47	56696.78	2.45	6.0 ± 0.0	5.4 ± 0.1	-0.6 ± 0.1	-8.52	16.87	1.72	0.80	0.00	2160
508	A	57185.17	57195.60	2.48	6.7 ± 0.1	6.3 ± 0.1	-0.5 ± 0.1	-5.25	4.93	-0.68	0.73	0.07	1300
508	A	57789.44	57805.35	3.78	7.1 ± 0.1	6.2 ± 0.1	-0.8 ± 0.1	-9.61	20.33	-0.62	0.87	0.00	2380
508	A	57805.35	57817.32	2.84	6.2 ± 0.1	6.6 ± 0.1	0.4 ± 0.1	4.29	4.27	-0.15	0.07	0.53	860
508	A	57874.21	57892.29	4.30	7.1 ± 0.1	6.5 ± 0.1	-0.6 ± 0.1	-6.03	4.95	0.45	0.87	0.00	1730
508	A	57901.21	57918.16	4.03	6.1 ± 0.1	3.5 ± 0.1	-2.6 ± 0.1	-22.34	105.26	-0.68	0.93	0.00	2810
508	A	57918.16	57933.42	3.63	3.5 ± 0.1	2.8 ± 0.1	-0.7 ± 0.1	-6.25	9.12	0.08	0.73	0.00	1510
509	B	56780.23	56782.25	0.55	4.4 ± 0.1	5.2 ± 0.1	0.8 ± 0.2	4.88	6.78	0.08	0.00	0.78	710
613	A	56686.47	56696.78	3.08	5.0 ± 0.1	5.4 ± 0.1	0.4 ± 0.1	4.26	4.57	0.15	0.00	0.44	540
613	A	56751.34	56755.34	1.19	5.1 ± 0.1	4.6 ± 0.1	-0.5 ± 0.1	-4.96	5.13	1.24	0.56	0.00	810
613	A	56772.23	56780.23	2.39	4.7 ± 0.1	4.1 ± 0.1	-0.6 ± 0.1	-7.28	8.76	1.00	0.88	0.00	1630
631	A	56783.25	56795.18	3.21	6.5 ± 0.1	7.2 ± 0.1	0.7 ± 0.2	4.37	6.73	1.28	0.15	0.46	470
717	A	56715.39	56717.33	0.61	17.3 ± 0.5	23.6 ± 0.7	6.2 ± 0.9	7.14	6.65	1.07	0.02	0.50	1690
717	A	56717.33	56720.45	0.98	23.6 ± 0.7	17.7 ± 0.6	-5.8 ± 0.9	-6.44	5.17	1.84	0.56	0.06	1690
722	A	57185.17	57195.60	2.94	10.5 ± 0.1	8.9 ± 0.2	-1.5 ± 0.2	-7.28	11.79	1.34	0.82	0.06	740
730	A	56751.34	56755.34	1.08	24.5 ± 0.1	23.5 ± 0.1	-0.9 ± 0.2	-5.08	5.17	-0.56	0.41	0.06	750
730	A	56755.34	56768.23	3.49	23.5 ± 0.1	24.6 ± 0.1	1.1 ± 0.2	6.11	4.20	0.41	0.04	0.49	1250
743	A	56715.39	56717.33	0.71	9.3 ± 0.5	12.7 ± 0.6	3.4 ± 0.7	4.52	4.92	0.54	0.10	0.43	320
743	A	56780.23	56782.25	0.74	12.7 ± 0.4	10.0 ± 0.4	-2.6 ± 0.6	-4.69	7.45	0.16	0.52	0.10	1610
770	A	56825.19	56829.21	1.41	3.2 ± 0.0	3.5 ± 0.0	0.3 ± 0.1	5.54	4.72	0.67	0.00	0.73	1580

Table 4.1 (cont'd)

RM ID	BAL ID	MJD_1 (days)	MJD_2 (days)	Δt_{rest} (days)	EW_1 (Å)	EW_2 (Å)	ΔEW (Å)	σ ($_{\Delta EW}$)	G_B	G_C	f (>1)	f (<−1)	Δv_{co} *
786	A	56683.48	56686.47	0.98	2.2 ± 0.1	1.6 ± 0.1	-0.6 ± 0.1	-5.03	6.42	1.56	0.67	0.00	590
786	B	56660.21	56664.51	1.42	31.9 ± 0.1	33.6 ± 0.2	1.8 ± 0.2	7.89	12.27	1.21	0.03	0.74	2290
786	B	56669.50	56683.48	4.60	34.3 ± 0.3	32.2 ± 0.1	-2.1 ± 0.3	-6.35	7.92	1.22	0.61	0.03	2590
786	B	56683.48	56686.47	0.98	32.2 ± 0.1	31.4 ± 0.1	-0.8 ± 0.2	-4.92	4.48	1.56	0.45	0.06	290
786	B	56686.47	56696.78	3.39	31.4 ± 0.1	32.8 ± 0.1	1.4 ± 0.2	9.17	13.20	0.38	0.00	0.71	3140
786	B	56717.33	56720.45	1.02	33.3 ± 0.1	32.6 ± 0.1	-0.7 ± 0.2	-4.58	4.99	0.84	0.52	0.10	1430
786	B	56745.28	56747.42	0.70	32.0 ± 0.1	33.3 ± 0.1	1.3 ± 0.1	8.73	15.19	-0.49	0.00	0.74	2290
786	B	56749.37	56751.34	0.65	33.7 ± 0.1	32.1 ± 0.1	-1.5 ± 0.2	-9.39	18.63	-0.89	0.77	0.03	3970
786	B	56772.23	56780.23	2.63	32.8 ± 0.1	33.5 ± 0.1	0.7 ± 0.1	5.66	7.68	-0.41	0.06	0.58	1140
786	B	56804.19	56808.26	1.34	32.6 ± 0.1	33.7 ± 0.1	1.2 ± 0.2	6.48	7.88	1.53	0.03	0.48	1710

*Velocity in units of km s^{-1}.

4.3 Causes of Variability

There are many different models for the drivers of variability of BALs. Previous studies have found that in some cases, the variability is consistent with models involving variations in the amount of ionizing radiation received by the gas (e.g., Filiz Ak et al. 2012, 2013; Capellupo et al. 2012), while other studies suggest that the observed variability is due to the transverse movement of the outflow material across our line of sight (often referred to as "cloud-crossing", e.g., Lundgren et al. 2007; Gibson et al. 2008; Hall et al. 2011; Vivek et al. 2012; Capellupo et al. 2013).

We can use various characteristics of BAL variability as well as the spectra themselves to assess the likelihood of one or the other of these mechanisms as the cause for our observed rapid variability. For example, the presence (or lack) of coordinated variability across the full profile of a BAL trough and between other C IV troughs at different velocities can provide evidence in support of (or against) the observed variability being caused by changes in the ionization state of the gas. The presence of BAL troughs of other species can provide information on whether or not the C IV BAL is saturated (e.g., Capellupo et al. 2017); saturated BAL troughs are unlikely to quickly respond to changes in ionizing continuum in the same manner as unsaturated troughs, which would lead one to favor cloud-crossing models to explain observed variability. We below examine various characteristics of our observed short-timescale BAL variability and the quasar spectra themselves to assess the evidence they provide in support of various physical models driving the variability.

4.3.1 Coordinated Variability Across the Width of Individual BAL Troughs

We first search for coordinated variability across individual BAL troughs. We assume that all (binned) pixels in a trough with $|\chi| < 1$ (χ characterizes the difference in flux between the two spectra) represent noise around an unchanging trough; we consider these pixels to be consistent with zero variability. For each rapidly-varying BAL, we measure the fraction of pixels in the BAL trough with $\chi > 1$, denoted $f(\chi > 1)$, and the fraction with $f(\chi < -1)$. The meaning of the

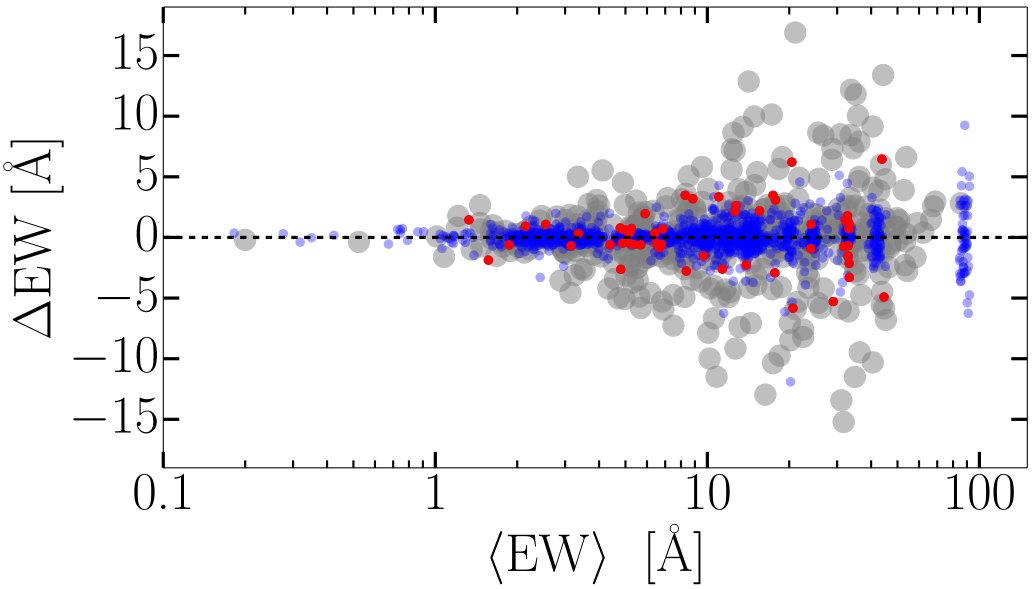

Figure 4.1 Sequential epoch ΔEW versus average EW for all pairs of spectra in our sample (blue dots) and our rapidly-varying pairs (red dots). Gray dots represent data from Filiz Ak et al. (2013), Barlow (1993), Lundgren et al. (2007), and Gibson et al. (2008) for comparison. $\langle EW \rangle$ is shown in log-scale. The horizontal blue line shows $\Delta\mathrm{EW} = 0$.

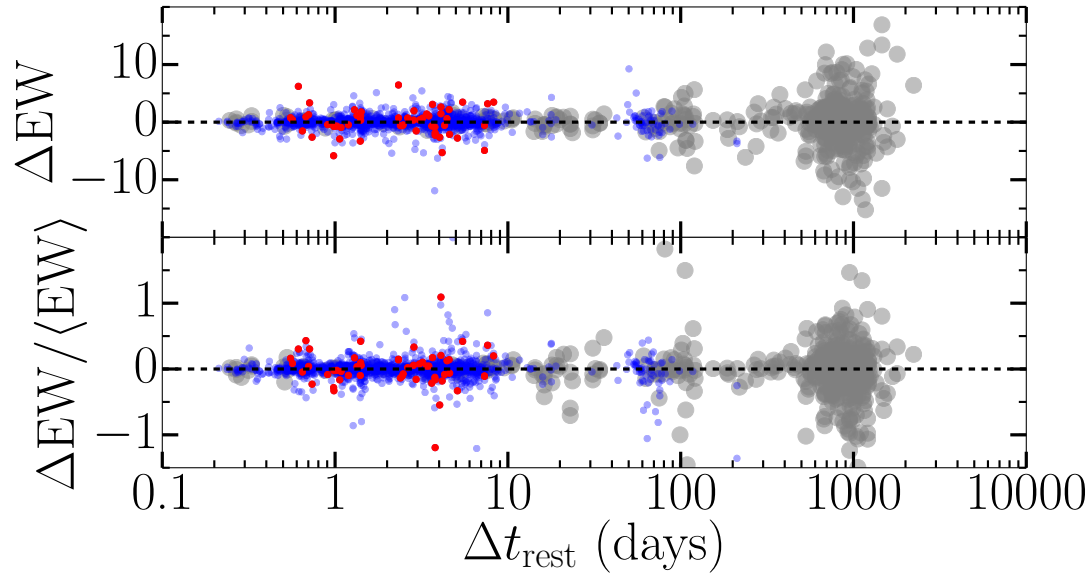

Figure 4.2 ΔEW and $\Delta\mathrm{EW}/\langle\mathrm{EW}\rangle$ versus rest-frame time difference for every sequential epoch pair of every object (blue dots) and for our pairs of epochs that are identified as rapidly-varying (red dots). Gray circles indicate data from Filiz Ak et al. (2013), Barlow (1993), Lundgren et al. (2007), and Gibson et al. (2008).

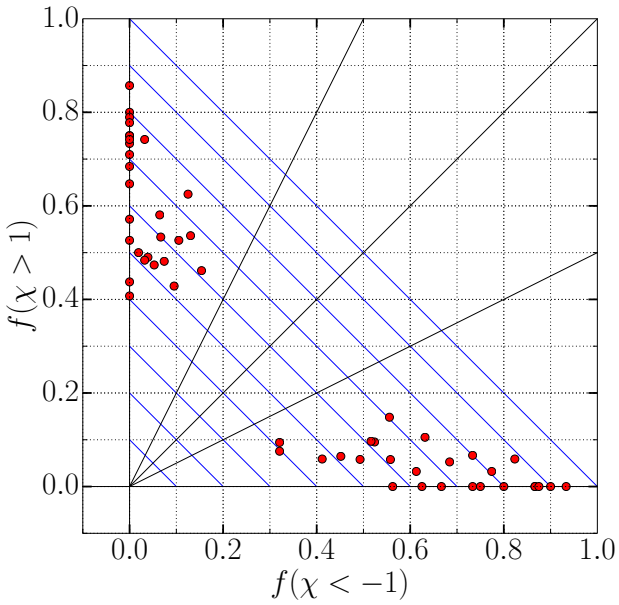

Figure 4.3 The fraction of pixels with $\chi > 1$ $f(\chi > 1)$ as a function of the fraction of pixels with $\chi < -1$ ($f(\chi < -1)$) for the epoch pairs showing rapid BAL variability (red circles). Black solid lines indicate ratios of 2:1, 1:1, and 1:2 to guide the eye, and the blue diagonals represent lines of constant $f(-1 < \chi < 1)$.

various possible combinations of these values can be summarized as follows:

1. High values of either $f(\chi > 1)$ or $f(\chi < -1)$ correspond to variability which is consistent with being coordinated in the same direction across a trough. Such variability is consistent with a model in which ionization variability is the cause of the observed changes in the BAL. These cases cannot be explained by crossing clouds alone because no model of such clouds has been proposed that can explain coordinated variability over thousands of km s^{-1} on timescales of days or less. There may be some cases where where part(s) of the trough vary in the same direction, but unequally (e.g., RM128 BAL[A] MJDs 56768–56772; see Figure Set 3.5). Such variability may be consistent with ionization variability with a range of densities across the outflow, or with ionization variability *and* crossing clouds — but again the variability cannot be explained by crossing clouds alone.

2. If χ is nonzero in parts of the trough and effectively zero in other parts, we are seeing variable and stable regions of the trough, respectively (e.g., RM 357 BAL[B] MJDs 56755–56768, RM 717 BAL[A] MJDs 56717–56720, or RM 786 BAL[B] MJDs 56745–56747). Such variability may be consistent with crossing clouds if the velocity widths of the variable regions are sufficiently small, but this behavior can also be explained in principle by ionization variability combined with saturation or different densities within the outflow itself.

3. If $f(\chi > 1)$ and $f(\chi < -1)$ are both significantly nonzero, we are seeing variability in both directions simultaneously (i.e., the BAL is weakening in some regions and strengthening in

some regions). Such variability may be consistent with crossing clouds or with ionization variability with a range of densities within the outflow.

Figure 4.3 shows $f(\chi > 1)$ vs. $f(\chi < -1)$ for our rapidly-varying pairs of spectra, and we provide $f(\chi > 1)$ and $f(\chi < -1)$ values in Table 4.1. BALs experiencing coordinated variability across the trough (the first situation described above) cluster along either the horizontal or vertical axis of Figure 4.3. Cases showing coordinated variability in the same direction across the majority of the trough (e.g., RM 508) appear farthest from the origin, and objects where part of the trough varies but the rest is consistent with no variability lie closer to the origin along the axes. BALs with significant variability in both directions (the third scenario described above) will lie close to a 45-degree line.

All of our cases lie between the vertical or horizontal axes and the lines indicating a 2:1 ratio between the two measured quantities. Most of the sets of measurements are consistent with situations (1) and (2) above, which suggest that ionization variability likely plays a role.

We see no cases representing the scenario (3) described above, where there is significant amounts of variability in both directions (i.e., part of the trough strengthens while another part weakens). However, we note that our aforementioned variability significance criteria select against such cases. Consider, for example, a scenario in which half of a BAL strengthens by some large amount, and the other half weakens by a similar amount. The ΔEW of such a case would approach zero. Thus, this case would not be flagged as significant by our $\sigma_{\Delta \mathrm{EW}} > 4$ criterion, although significant variability could exist in the individual regions within the BAL. Such preferential selection could explain the overabundance of coordinated variability presented in Figure 4.3.

We also measured the largest number of contiguous pixels in each trough with $\chi > 1$ and $\chi < -1$ and denote this quantity as v_{co} — this value is the largest velocity width with "coordinated" variability that a model of variability will need to explain. These numbers are provided in Table 4.1 for each pair of epochs. There is a large range of v_{co} within our sample, ranging from just under 300 km s^{-1} to just under 4000 km s^{-1}, indicating a wide variety of coordinated velocity widths. More than half of the epoch pairs show coordinated variability in regions >1000 km s^{-1}.

Large regions of coordinated variability can be easily explained by ionization variability — models that rely on cloud-crossing scenarios must be able to explain coordinated variability across these velocity widths.

4.3.2 Coordinated Variability Between Additional CIV BALs

Seven of our 15 quasars hosting rapidly varying BALs (RM 128, 217, 257, 357, 509, 730, and 786) have additional C IV BALs present in their spectra at different velocities. These quasars provide an opportunity to search for coordination between rapidly varying C IV troughs with those at different velocities — such coordination was reported by Capellupo et al. (2012), Filiz Ak et al. (2012, 2013), and De Cicco et al. (2018) on longer time baselines. For all pairs of epochs where at least one of the BALs experienced significant rapid variations, we also explore the behavior of the other BAL during that same time period. Figure 4.4 shows ΔEW for the two C IV BALs compared with one another for all of the significantly-variable epoch pairs with two BALs present. In addition, the behavior of the additional C IV BALs can be compared to the rapidly-varying BALs using Figure Sets 3.2 and 3.5.

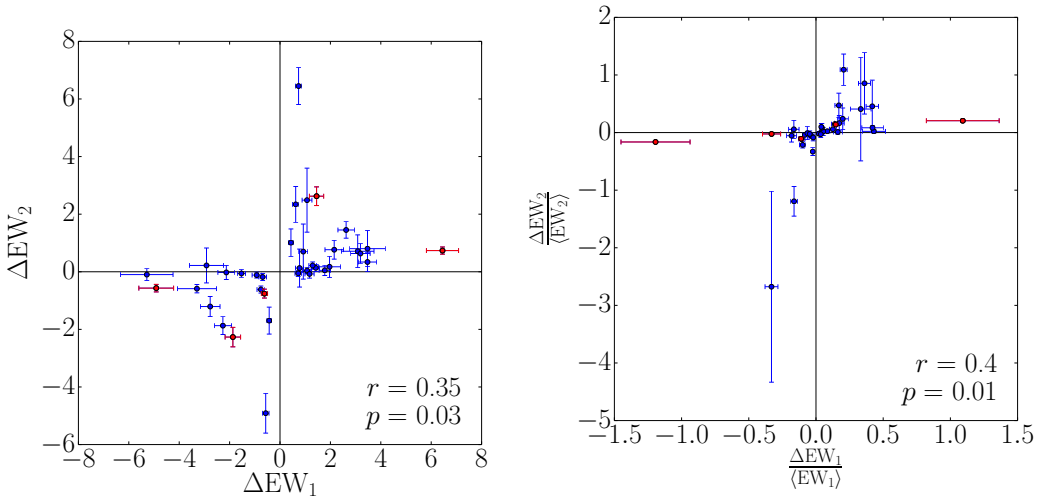

Figure 4.4 ΔEW (top panel) and ΔEW/$\langle$EW$\rangle$ (bottom panel) of accompanying C IV BALs as a function of the ΔEW of the rapidly-varying BALs. In all cases, ΔEW_1 refers to the measurement of the BAL that is identified as rapidly-variable, and ΔEW_2 refers to the accompanying BAL during the same pair of epochs. Blue points represent pairs where only one of the BALs (ΔEW_1) passed our criteria for rapid variability; in these cases, the second BAL varied with a lower significance (or is sometimes statistically consistent with zero variability). Red points represent pairs of epochs where both BALs varied significantly. The results of a Pearson correlation test are provided in the lower-right corner of each subplot; r is the measured Pearson coefficient and p is the corresponding probability that the measured r would be obtained randomly if the two quantities were actually uncorrelated.

We have 36 pairs of spectra with at least one BAL identified as rapidly-varying in quasars hosting a second BAL. A detailed discussion of each individual object and its additional C IV BAL is provided in the Appendix.

Figure 4.4 shows a potential correlation between ΔEW of the two C IV troughs. This provides tentative evidence for coordinated variability between the two troughs in many cases. We also performed a Pearson correlation test to determine the strength of the correlation between the two quantities, computing the Pearson correlation coefficient r and the corresponding probability p that describes the likelihood of obtaining the measured r value if the two quantities are actually uncorrelated. We obtain $r = 0.35$ and $p = 0.03$ for ΔEW changes and $r = 0.4$ and $p = 0.01$ for ΔEW/$\langle$EW$\rangle$, indicating that the EW changes of the two C IV troughs are mildly correlated. We interpret this as tentative evidence for coordinated variability between C IV BAL troughs in our sample.

4.3.3 SiIV and AlIII

Recent work has demonstrated that the presence of BALs at velocities corresponding to the C IV BAL but arising from other absorption species can provide clues to the physical properties of the BAL outflows (e.g., Filiz Ak et al. 2014; Capellupo et al. 2017). To investigate this, Filiz Ak

et al. (2014) divided their sample of C IV BALs into categories according to the presence of other species: If neither Si IV$\lambda\lambda$1393, 1403 nor Al III$\lambda\lambda$1855, 1863 is present at velocities corresponding to an identified C IV BAL, said BAL is denoted a C IV$_{00}$ trough. If a Si IV BAL is present but Al III is not detected, it is denoted as a C IV$_{S0}$ trough (or C IV$_{s0}$ if it is a mini-BAL), and if both Si IV and Al III BALs are present at corresponding velocities, it is denoted as a C IV$_{SA}$ trough (or C IV$_{sa}$ if they are both mini-BALs rather than formal BALs and C IV$_{Sa}$ if the Si IV feature is a formal BAL but the Al III feature is a mini-BAL). In a sample of 851 BAL troughs, they find that 13$\pm$1% of their BAL troughs fall into the C IV$_{00}$ category, 61$\pm$3% of their sample falls into the C IV$_{S0}$ or C IV$_{s0}$ category, and 26$\pm$1% of their sample falls into the C IV$_{SA}$, C IV$_{Sa}$, or C IV$_{sa}$ category.

We visually inspected the mean spectra of our quasars to determine whether or not these additional species are present in our sample, and assigned each BAL a category following Filiz Ak et al. (2014), with one notable change: We do not differentiate between BALs and mini-BALs when considering Si IV and Al III. We thus place our BAL troughs into only three categories (C IV$_{00}$, C IV$_{S0}$, and C IV$_{SA}$) as long as a BAL or mini-BAL of the other species is present. In some cases, there was slight evidence for absorption of Si IV or Al III that was not deep enough to meet the normalized flux threshold of 0.9 used in BAL searches, and thus the absorption is considered undetected. Our classifications for all identified BALs are given in Table 3.2. Please see the Appendix for details on individual objects. There are three cases in our BAL trough sample where there is not sufficient coverage of the Si IV region to determine a class — we denote these as C IV$_{N0}$ troughs in Table 3.2.

In our sample of 34 troughs with coverage of the Si IV region, we find 15 C IV$_{00}$ troughs (44^{+15}_{-11}% of our sample), 13 C IV$_{S0}$ troughs (38^{+14}_{-11}%), and six C IV$_{SA}$ troughs (18^{+11}_{-7}%). Among only our 19 rapidly-varying BAL troughs, we observe a distribution that is consistent with our full sample: Nine (50^{+23}_{-16}%) of the 18 BALs with short-term variability and Si IV coverage fall into the C IV$_{00}$ category, six (33^{+20}_{-13}%) of the BALs fall into the C IV$_{S0}$ category, and three BALs (17^{+16}_{-9}%) fall into the C IV$_{SA}$ category (the remaining rapidly-varying BAL, RM 361 BAL[A], does not have wavelength coverage of the Si IV region).

When a deep Si IV trough accompanies the observed C IV trough, the C IV trough must be heavily saturated given the relative cosmic abundances of Si and C and the relative ionic abundances expected in BAL outflows (e.g., Figure 4 of Hamann et al. 2000). More than half of our BAL troughs show accompanying Si IV, which indicates saturation and suggests that cloud-crossing likely plays a part in the observed variability in many of our BALs, as saturated troughs will not respond to changes in the incident ionizing flux in the same manner as unsaturated troughs.

However, the presence of saturated C IV troughs is not necessarily solid evidence for simple cloud-crossing scenarios. For example, consider RM 257 BAL [A], a C IV$_{SA}$ trough with two pairs of epochs where it is identified as rapidly-variable. The BAL shows coordinated variability across velocities of $\sim$3600 km s^{-1} and $\sim$7250 km s^{-1} (about 20% and 40% of the entire trough width). This quasar also contains a second, lower-velocity BAL that varies significantly in the same direction as this BAL. Coordinated variability of such a C IV trough over a velocity range too wide to be explained by cloud crossing indicates inhomogenous partial covering of some type; that is, different parts of the quasar emission regions are covered by absorbers of different optical depths along our sight-line (e.g., de Kool et al. 2002, Arav et al. 2005, Sabra & Hamann 2005). For example, the optical depth values might follow a power-law distribution (e.g., Arav et al. 2008), with a large fraction of the emitting area covered by gas optically thick in C IV and a small fraction covered by optically thin gas. Variations in the ionizing continuum leading to variations in the optical depth values would yield a more detectable change in residual flux from the emitting area

covered by optically thin gas than from the emitting area covered by optically thick gas. A BAL outflow exhibiting inhomogeneous partial covering therefore can exhibit strong Si IV and even P V absorption in a trough which nonetheless exhibits variability in the C IV equivalent width. Simultaneously modeling the variability of C IV and Si IV in such cases may constrain inhomogeneous partial convering models; however, we defer such detailed analysis to a future work.

PV

We also searched for P V$\lambda\lambda$1112,1118 absorption in our significant-variability sample. P V is a lower-abundance ion that has an ionization energy similar to that of C IV, and its presence, like that of Si IV, indicates that the corresponding component of their C IV absorption is highly saturated (e.g., Capellupo et al. 2017). There have been differing reports on the frequency of P V BALs; Capellupo et al. (2017) report that only 3-6% of BAL quasars examined show detectable P V, while Filiz Ak et al. (2014) estimate that about half of their sample contains visible signs of P V absorption. The incidence of detectable P V rises when other species such as Si IV or Al III are present — Filiz Ak et al. (2014) report that 88% of their C IV$_{\rm SA}$ troughs show detectable P V, about half of the C IV$_{\rm S0}$ troughs show detectable P V, and only 12% of C IV$_{00}$ troughs are accompanied by P V absorption.

In the cases in which the P V region is covered by our spectra, it falls toward the very blue end of the spectrum, which often contains significant noise, causing difficulties in its reliable detection, and this difficulty is compounded by the fact that it falls within the Lyα forest. A detailed analysis is thus beyond the scope of this work — however, we visually inspected the spectra for signs of broad P V absorption that corresponds to the velocities of our 37 identified CIV BALs. The results for each identified BAL in our entire sample are presented in Table 3.2. Only 15 of our 37 BALs have coverage of the P V region at corresponding velocities; for these 15 C IV BALs, we find tentative signs of accompanying P V in six cases (40^{+23}_{-15}%).

Three of the six likely P V BALs accompany rapidly-varying C IV BALs — in quasars RM 257, RM 631, and RM 730. All three also contain Si IV absorption (RM 631 and RM 730 are both C IV$_{\rm S0}$ troughs and RM 257 BAL[A] is a C IV$_{\rm SA}$ trough), further supporting saturation. One would thus expect that our observed variability is most likely due to cloud-crossing or, as discussed above, (Section 4.3.3), by inhomogeneous partial covering scenarios. The lack of substantial coordinated variability in these troughs (see the Appendix for details) is also consistent with these interpretations.

Chapter 5

Conclusion

5.1 Summary

We systematically searched for short-timescale (< 10-day) variability in a sample of 37 distinct C IV BALs in 27 unique quasars using data from the SDSS-RM program, which contains a large number of spectral epochs at a high cadence compared to previous studies of BAL variability. We further examine these spectra to evaluate potential models for the variability mechanisms and compare our observed variability to previous sample studies (e.g., Filiz Ak et al. 2013). Our major findings are the following:

1. We found 54 cases of significant rapid variability in 19 unique BALs (see Section 4.1) in 15 out of the 27 quasars in our sample (55^{+18}_{-11} %). This result demonstrates that short-term BAL variability is common; it has not been observed frequently in the past likely because high-SN observations intensively probing these short timescales did not exist. These quasars and their BAL troughs do not appear to be unique; their properties are similar to those of the general quasar population. See Section 4.1.
2. We compare the overall variability properties of our sample (ΔEW and fractional ΔEW) to previous studies to determine whether our rapid variability is unusual or more extreme than previously reported. The amplitude of variability in our sample does not appear to differ qualitatively from that previously observed (see Section 4.2).
3. We searched for coordinated variability across our rapidly-varying C IV BAL troughs and find that the velocities over which the variability is coordinated ranges from $\sim$290 km s^{-1} to $\sim$7250 km s^{-1} within the troughs. More than half of our troughs show coordinated variations across velocities $>$1000 km s^{-1} (see Section 4.3.1). This result is consistent with much of the observed variability being caused by changes in ionization state of the gas, which naturally explains coordinated variability across a range of velocities. However, many of our troughs show much smaller ranges of coordinated variability, suggesting that cloud-crossing may be responsible for the variability in other cases.
4. We see tentative evidence for coordinated variability between C IV troughs in quasars hosting more than one C IV BAL (see Section 4.3.2). This observation again indicates that the variability cannot be explained solely by a cloud-crossing scenario, as coordinated variability at such a large spread of velocities is difficult to achieve in the context of cloud-crossing models.
5. We investigate the presence of other BAL species such as Si IV, Al III, and P V in our sample and find that many of our C IV BALs are saturated; in these cases, cloud-crossing scenarios are more likely to be the cause for our observed rapid variability. See Section 4.3.3.

Previous sample studies of BAL variability have all found significant variability on all timescales explored; we similarly find significant BAL variability down to timescales of less than a day in the quasar rest frame. Our results suggest that future observational studies of BAL variability on longer timescales need to consider the likely possibility that the BALs have experienced significant variations, perhaps in many directions, within the time span between observations. In addition, models describing BAL formation and variability need to explain short-timescale variability to be viable, as such rapid variability is not a unique, extreme event, but appears to be common among quasars.

5.2 Future Work

Our study is the first to examine short BAL variability timescales (down to less than a day in the quasar rest frame) intensively for many different quasars. However, additional time-domain spectroscopic studies of quasars will be extremely useful in helping to expand our sample of quasars searched and to place better constraints on the frequency of such variability. Future high-cadence, high-SN studies of BAL variability will be crucial in uncovering the driving force behind this variability and the relevant applications to models of quasar outflows.

Bibliography

Ahn, C. P., Alexandroff, R., Allende Prieto, C., et al. 2014, ApJS, 211, 17

Arav, N., Kaastra, J., Kriss, G. A., et al. 2005, ApJ, 620, 665

Arav, N., Moe, M., Costantini, E., et al. 2008, ApJ, 681, 954

Barlow, T. A. 1993, PhD thesis, California University

Blanton, M. R., Bershady, M. A., Abolfathi, B., et al. 2017, AJ, 154, 28

Capellupo, D. M., Hamann, F., Shields, J. C., Halpern, J. P., & Barlow, T. A. 2013, MNRAS, 429, 1872

Capellupo, D. M., Hamann, F., Shields, J. C., Rodríguez Hidalgo, P., & Barlow, T. A. 2011, MNRAS, 413, 908

—. 2012, MNRAS, 422, 3249

Capellupo, D. M., Hamann, F., Herbst, H., et al. 2017, MNRAS, 469, 323

Cardelli, J. A., Clayton, G. C., & Mathis, J. S. 1989, ApJ, 345, 245

Dawson, K. S., Schlegel, D. J., Ahn, C. P., et al. 2013, AJ, 145, 10

Dawson, K. S., Kneib, J.-P., Percival, W. J., et al. 2016, AJ, 151, 44

De Cicco, D., Brandt, W. N., Grier, C. J., et al. 2018, ArXiv e-prints, arXiv:1804.04666

de Kool, M., Korista, K. T., & Arav, N. 2002, ApJ, 580, 54

Di Matteo, T., Springel, V., & Hernquist, L. 2005, Nature, 433, 604

Eisenstein, D. J., Weinberg, D. H., Agol, E., et al. 2011, AJ, 142, 72

Filiz Ak, N., Brandt, W. N., Hall, P. B., et al. 2012, ApJ, 757, 114

—. 2013, ApJ, 777, 168

—. 2014, ApJ, 791, 88

Gehrels, N. 1986, ApJ, 303, 336

Gibson, R. R., Brandt, W. N., Gallagher, S. C., Hewett, P. C., & Schneider, D. P. 2010, ApJ, 713, 220

Gibson, R. R., Brandt, W. N., Gallagher, S. C., & Schneider, D. P. 2009a, ApJ, 696, 924

Gibson, R. R., Brandt, W. N., & Schneider, D. P. 2008, ApJ, 685, 773

Gibson, R. R., Jiang, L., Brandt, W. N., et al. 2009b, ApJ, 692, 758

Grier, C. J., Hall, P. B., Brandt, W. N., et al. 2015, ApJ, 806, 111

Grier, C. J., Brandt, W. N., Hall, P. B., et al. 2016, ApJ, 824, 130

Gunn, J. E., Siegmund, W. A., Mannery, E. J., et al. 2006, AJ, 131, 2332

Haggard, D., Arraki, K. S., Green, P. J., Aldcroft, T., & Anderson, S. F. 2012, in Astronomical Society of the Pacific Conference Series, Vol. 460, AGN Winds in Charleston, ed. G. Chartas, F. Hamann, & K. M. Leighly, 98

Hall, P. B., Anosov, K., White, R. L., et al. 2011, MNRAS, 411, 2653

Hall, P. B., Sadavoy, S. I., Hutsemekers, D., Everett, J. E., & Rafiee, A. 2007, ApJ, 665, 174

Hamann, F. W., Netzer, H., & Shields, J. C. 2000, ApJ, 536, 101

Higginbottom, N., Proga, D., Knigge, C., et al. 2014, ApJ, 789, 19

King, A., & Pounds, K. 2015, Annual Review of Astronomy and Astrophysics, 53, 115

Lundgren, B. F., Wilhite, B. C., Brunner, R. J., et al. 2007, ApJ, 656, 73

Moll, R., Schindler, S., Domainko, W., et al. 2007, A&A, 463, 513

Murray, N., Chiang, J., Grossman, S. A., & Voit, G. M. 1995, ApJ, 451, 498

Pâris, I., Petitjean, P., Aubourg, É., et al. 2018, A&A, 613, A51

Park, D., Woo, J.-H., Denney, K. D., & Shin, J. 2013, ApJ, 770, 87

Pei, Y. C. 1992, ApJ, 395, 130

Proga, D. 2000, ApJ, 538, 684

Richards, G. T., Strauss, M. A., Fan, X., et al. 2006, AJ, 131, 2766

Sabra, B. M., & Hamann, F. 2005, ArXiv Astrophysics e-prints, astro-ph/0509421

Schlafly, E. F., & Finkbeiner, D. P. 2011, ApJ, 737, 103

Schneider, D. P., Richards, G. T., Hall, P. B., et al. 2010, AJ, 139, 2360

Shen, Y. ., Brandt, W. N., Richards, G. T., et al. 2018, ApJ, in preparation

Shen, Y., Brandt, W. N., Dawson, K. S., et al. 2015, ApJS, 216, 4

Smee, S. A., Gunn, J. E., Uomoto, A., et al. 2013, AJ, 146, 32

van der Marel, R. P., & Franx, M. 1993, ApJ, 407, 525

Vanden Berk, D. E., Richards, G. T., Bauer, A., et al. 2001, AJ, 122, 549

Vivek, M., Srianand, R., Mahabal, A., & Kuriakose, V. C. 2012, MNRAS, 421, L107

Welling, C. A., Miller, B. P., Brandt, W. N., Capellupo, D. M., & Gibson, R. R. 2014, MNRAS, 440, 2474

Weymann, R. J., Morris, S. L., Foltz, C. B., & Hewett, P. C. 1991, ApJ, 373, 23

White, R. L., Becker, R. H., Helfand, D. J., & Gregg, M. D. 1997, ApJ, 475, 479

Appendix

We here provide additional information and notes on the individual sources in our quasar sample.

RM 039

RM 039 hosts an extremely broad, deep C IV BAL, and also contains deep Si IV and Al III BALs, placing it into the C IV$_{\rm SA}$ category. This object also has a P V BAL at corresponding velocities, indicating that the C IV BAL is highly saturated in this object.

RM 073

RM 073 contains two C IV BALs, neither of which are identified to be significantly variable on short timescales. There is no evidence for corresponding Si IV or Al III BALs or mini-BALs.

RM 116

RM 116 formally has two distinct C IV BALs identified; however, visual inspection of the mean spectrum suggests that these two BALs may belong to the same absorption system. There also exists a Si IV absorption feature, and a very meager accompanying Al III trough. However, this though trough is too small to be considered a true absorption feature.

RM 128

RM 128 has two BALs, both identified as rapidly-varying but on different dates. In all four epochs exhibiting short-timescale variability, the other BAL also experiences an EW shift in the same direction, but at a lower significance. We interpret this as tentative evidence for coordinated variability, although the low significance of the secondary BAL variability prohibits a definite conclusion. The higher-velocity BAL in RM 128 (BAL[A]) also has a corresponding Si IV BAL as well as slight evidence for shallow Al III absorption at the same velocities. The lower-velocity BAL[B] does not appear to have any accompanying Si IV or Al III absorption.

RM 155

Our spectra for RM 155 do not have complete coverage of the Si IV region; however, we see evidence for the beginning of a Si IV trough at corresponding velocities to the very deep C IV BAL, as well as a strong Al III absorption feature. Thus, this is a C IV$_{SA}$ quasar.

RM 195

When searching for additional C IV BALs in RM 195, we identified a higher-velocity candidate trough that is just short of the "formal" BAL width criterion of 2000 km s^{-1} due to noise within the trough. There exists evidence for an accompanying Si IV feature to this higher-velocity trough; however, the BAL that is formally identified shows no accompanying Si IV or Al III absorption.

We also note that RM 195 has another formal C IV BAL at higher outflow velocities that was excluded from our sample due to the presence of sky line contamination (see Section 3.1).

RM 217

This quasar has two identified C IV BALs, but only is identified as rapidly-varying. The high-velocity BAL[A] shows less significant variability —in two epoch pairs, however, the less-significant variability is in the same direction as the significant variability. In one epoch pair, the EW of BAL[A] changes in the opposite direction, and it has disappeared completely in the last epoch pair. This quasar is one of two that harbors a high-velocity BAL (BAL[A]) that disappears during the campaign. Additionally, this quasar has Si IV BALs present at velocities corresponding to both C IV BALs, although no Al III absorption is visible.

RM 257

RM 257 has two BALs, both identified as rapidly-varying. BAL[A] only has two epoch pairs identified as rapidly-varying (MJDs 57510-57518 and 57518-57544). BAL[B] is also significantly variable in the same direction during these epoch pairs. In the additional three epoch pairs that BAL[B] is identified as rapidly variable, BAL[A] also varies in the same direction, but the variability is significant at less than 4σ. Thus, we again find tentative evidence for coordinated variability.

RM 257 BAL[A] has accompanying Si IV and Al III troughs. The P V region corresponding to these velocities is cut off at the blue end of the wavelength region, but the spectrum does appear to have P V absorption.

RM 284

RMID 284 shows broad C IV absorption within our search range — however, this quasar also has a high-velocity C IV trough extending from approximately 35,000 to 59,000 km s^{-1} with a maximum depth of approximately 50% of the continuum flux. The absorption EW has generally decreased from 2014 to 2017, but the maximum depth has not. There is accompanying N V absorption at the lowest trough velocities visible at the extreme blue edge of the SDSS-RM spectrum, but we lack coverage of the P V region at these velocities. The strength of any accompanying Si IV absorption in this quasar is impossible to determine without detailed continuum modeling of the Lyα/N V emission region, so we assign the C IV$_{N0}$ designation to this target to indicate this uncertainty. There does not appear to be substantial Al III absorption, although the region blueward of Al III has considerable contamination and blending, making it difficult to interpret the spectrum.

RM 339

RM 339 contains BAL troughs in both Si IV and Al III at similar velocities to the C IV trough. Thus, this is a C IV$_{SA}$ quasar.

RM 357

RM 357 has two C IV BALs troughs. BAL[A], the higher-velocity BAL, displays rapid variability on two separate occasions. On both of those occasions, BAL[B] also exhibits rapid variability in the same direction. BAL[B] shows rapid variability in five additional epoch pairs as well, but in two of these pairs, BAL[A] has disappeared entirely. In the epoch pairs where BAL[A] remains present, it varies in the same direction as BAL[B], but at a lower significance. Thus, we yet again see tentative evidence for coordinated variability.

RM 357 BAL[B] has accompanying Si IV absorption, but no signs of Al III features. The P V region is not covered by our spectra for this quasar.

RM 361

RM 361 has single, deep BAL trough. The Si IV region is not covered by our spectra, so we assign this BAL to the C IV$_{N0}$ category. There is not strong evidence for Al III absorption.

RM 408

RM 408 has visible absorption at velocities corresponding to the C IV BAL[A]; however, both of these features are too narrow to meet our formal BAL definition, so we assign this BAL to the C IV$_{00}$ category. We do not have coverage of the P V region in this object.

RM 508

This quasar exhibits C IV absorption with no accompanying Si IV, Al III, or P V features. Additional C IV absorption is visible at lower velocities that is both slightly and narrow to meet our formal BAL definition. The C IV BAL[A] in this target varies significantly on short timescales, sometimes with exceptionally high significance (i.e., greater than $20\sigma_{\Delta \mathrm{EW}}$), making this quasar especially noteworthy.

RM 509

RM 509 has two C IV BALs, but only the lower-velocity BAL[B] is rapidly variable. This variability only occurs in a single pair of epochs. Between this rapidly-varying epoch pair, BAL[A] varies in the same direction but at lower significance. The higher-velocity BAL[A] has an accompanying Si IV trough, but no Al III feature; the lower-velocity BAL[B] shows no BALs or mini-BALs of either species. There is no conclusive evidence for a P V BAL in this target.

RM 564

This source has a high-velocity C IV BAL with accompanying Si IV absorption, but no Al III feature. We also see a significant lower-velocity feature in the Si IV region that must be an extremely high-velocity C IV trough.

RM 565

The spectra for RM 565 barely clear our SN threshold; it is thus difficult to identify different species throughout the spectra. However, we identify two BALs: The velocities covered by BAL[A] are not fully covered by the spectra, so we are unsure if Si IV is present at these velocities. Al III does not appear to be present in the spectra. The lower-velocity BAL[B] appears to have accompanying Si IV absorption, but no Al III absorption.

RM 613

RM 613 has one C IV BAL that meets the formal BAL definition, although there is an additional lower-velocity mini-BAL. Si IV absorption is likely present at velocities corresponding to the BAL, but, at $<10\%$ of the continuum flux, it does not formally meet the definition of a BAL. There is no evidence for accompanying Al III absorption. This quasar was investigated by Grier et al. (2015), which reported the first detection of significant BAL variability on timescales shorter than five days in the quasar rest frame. Their investigation revealed four different pairs of spectra separated by less than rest-frame days that exhibited $> 4\sigma_{\Delta \mathrm{EW}}$ BAL variability. We find qualitatively similar results (i.e., the BAL varies on short timescales); however, we identify slightly different pairs of epochs due to differences in the continuum/emission-line fits and the implementation of our additional variability significance criteria (i.e, the use of our G statistic). We again stress our goal of assembling a clean, conservative collection significant BAL variations, and our strict significance criteria could eliminate a few epoch pairs that may exhibit true variability.

RM 631

This quasar has a C IV BAL accompanied by Si IV absorption. Additionally, a Al III absorption feature exists, but it does not drop down below a normalized flux density of 0.9. Thus, this is a C IV$_{S0}$ BAL. However, strong evidence for Al III exists, and evidence for P V is apparent as well.

RM 717

RM 717 exhibits a broad C IV BAL with multiple components; we see a similar structure in the accompanying Si IV BAL at corresponding velocities. Hints of possible similarly-structured Al III absorption are visible, but the flux does not drop below 0.9 at any point. Thus, this feature cannot definitely be considered an Al III BAL.

RM 722

This object displays a single C IV BAL with no accompanying Si IV or Al III absorption, though there are traces of lower-velocity Si IV features superimposed on the Si IV emission line. These fea-

tures are likely too narrow to be considered BALs or mini-BALs, however.

RM 729

RM 729 contains a fairly deep C IV BAL trough with accompanying Si IV absorption and traces of accompanying Al III absorption. The Al III absorption is not quite deep enough to be considered a formal BAL or mini-BAL. There is potential evidence for a P V BAL feature, though the low SN in the P V region makes this uncertain.

RM 729 also has a second formal C IV BAL present in its spectrum at higher velocity; however, it was excluded from our study due to contamination by bad pixels (see Section 3.1).

RM 730

RM 730 possesses two C IV BALs. The higher-velocity BAL[A] shows significant short-term variability in two pairs of epochs; BAL[B] in this object does not vary significantly over these time periods. BAL[A] shows coordinated variability on velocity scales of 750 and 1250 km s^{-1} (only about 5% and 9% of the entire trough width) during the two identified epoch pairs. There is a Si IV BAL present at velocities corresponding to BAL[A], and traces of Al III absorption, but the Al III features are too shallow to be considered BALs; we thus place this object into the $\mathrm{C\,IV_{S0}}$ category. There is no evidence for Si IV, Al III, or P V BALs or mini-BALs at velocities corresponding to the lower-velocity BAL[B].

RM 743

RM 743 has strong C IV, Si IV, and Al III BAL features present. In addition, Al IIλ1670 absorption also appears in this quasar.

RM 770

This quasar shows potential Si IV absorption corresponding to BAL[A], but no Al III features.

RM 785

This source has a single C IV BAL, accompanied by likely Si IV absorption. There are potential P V BALs at corresponding velocities, although the low SN of the region makes this a tentative interpretation.

RM 786

RM 786 has a very shallow high-velocity BAL[A] that varies rapidly for one epoch pair. For the same epoch pair, the low-velocity, deeper BAL[B] varies in the same direction, suggesting coordinated variability between the two. BAL[B] varies significantly on many more epochs, however — sometimes BAL[A] varies in the same direction, but for two epoch pairs, the troughs vary in opposite directions. Again, we note that the BAL[A] is varying at low significance in these cases, so the disagreement is tentative rather than conclusive.

Zach Hemler

zqh5104@psu.edu ∗ (717) 579-3073 ∗ 1803 Charles St, New Cumberland, PA 17070

EDUCATION

The Pennsylvania State University
Bachelor of Science ***(Honors)***, Astronomy & Astrophysics
Expected August 2018

RESEARCH & EXPERIENCE

Undergraduate Researcher January 2016 - Present
The Pennsylvania State University
Supervisors: Profs. Niel Brandt & Donald Schneider
- Leading a sample study of gas outflow kinematics and variability in SDSS quasars
- Collaborating with team of 8+ faculty members at several institutions
- Developing Python scripts to fit and analyze AGN spectra via computational methods
- Employing Matplotlib to create many plots of any sort – *If you got it, I'll plot it!*

SciCoder 8: Workshop Attendee August 2016
Yale University
- Introduced to graduate-level programming practices and tools of astronomy
- Gained experience with version control software (Git)
- Designed, populated, and queried databases using SQLite and Python
- Familiarized with statistical computing (R)
- Acquainted with multiprocessing and unit testing concepts

PUBLICATIONS

"The Sloan Digital Sky Survey Reverberation Mapping Project: Investigations of Short-Timescale Broad Absorption Line Variability" **Hemler, Z.S.**, Grier, C.J., Brandt, W.N., Hall, P.B., Horne, K., Schneider, D.P., et al. 2018
[In Preparation]

OUTREACH & PRESENTATIONS

AAS Poster Presenter January 2018
"Investigations of Short-Timescale Outflow Variability in Quasars of the Sloan Digital Sky Survey," **Hemler, Z.S.**, Grier, C.J., Brandt, W.N., Hall, P.B., Schneider, D.P., et al. 2018, American Astronomical Society Meeting Abstracts #231, #250.36

Undergraduate Poster Presenter October 2017
Eberly College of Science Undergraduate Poster Exhibition

Guest Instructor June 2017
Computers in the Universe: A PSU In-Service Workshop in Astronomy
- Delivered lecture on the computational basics of fractals and self-similarity
- Wrote interactive fractal-generating program and trained attendees in its use

Key-Holding Member April 2013 - August 2015
Astronomical Society of Harrisburg
- Operated telescopes and explained astrophysical concepts to public visitors

SKILLS

Languages: Python, IDL, MATLAB, C++
Packages: NumPy, Matplotlib, AstroPy, SciPy, pandas
Applications: Git, SQLite, DS9, MaxIm DL, Microsoft Excel
Operating Systems: Unix, Linux, Mac OSX, Windows

GRANTS & AWARDS

NSF REU Grant	March 2017
Evan Pugh Scholar Junior Award	March 2017
Eberly Undergraduate Research Grant	December 2016
Kadtke Scholarship	July 2016
NSF REU Grant	May 2016
President Sparks Award	April 2016
President's Freshman Award	April 2015
Academic Excellence Scholarship	August 2014

COURSES COMPLETED

ASTRO 410: Computational Astrophysics (3)*
PHYS 430: Computational Physics (3)
ASTRO 480: Nebulae, Galaxies, and Cosmology (3)
ASTRO 485: High Energy Astrophysics (3)*
PHYS 479: Special and General Relativity (3)
ASTRO 451: Astronomical Techniques (3)
MATH 406: Advanced Calculus II (3)
MATH 405: Advanced Calculus I (3)
ASTRO 475W: Stars and Galaxies (3)
PHYS 400: Intermediate Electricity & Magnetism I (4)*
PHYS 410: Introduction to Quantum Mechanics I (4)*
PHYS 419: Theoretical Mechanics (3)*
ASTRO 320: Observational Astronomy Laboratory (2)*
ASTRO 292: Astronomy of the Distant Universe (3)
ASTRO 291: Astronomical Methods and the Solar System (3)
**: Honors*

REFERENCES

Prof. Niel Brandt
Verne M. Williaman Prof. of Astronomy & Astrophysics, PSU
Email: wnbrandt@gmail.com
Phone: (814) 865-3509

Prof. Donald Schneider
Department Head and Distinguished Prof. of Astronomy & Astrophysics, PSU
Email: dps7@psu.edu
Phone: (814) 863-9554

Dr. Catherine Grier
Postdoctoral Research Associate, PSU
Email: grier@psu.edu
Phone: (814) 867-1281